Title.

Numerical study on the effect of rotation radius of geotechnical centrifuge on the dynamic behavior of liquefiable sloping ground

Author names and affiliations.

Anurag Sahare[1], Yoshikazu Tanaka[2], Kyohei Ueda[2*]

[1]*Graduate School of Engineering, Kyoto University, Kyoto daigaku-katsura, Nishikyo-ku, Kyoto, 615-8530 Japan*

[2]*Disaster Prevention Research Institute, Kyoto University, Gokasyo, Uji, Kyoto, 611-0011 Japan*

***Corresponding autho**r

E-mail address: ueda.kyohei.2v@kyoto-u.ac.jp (Kyohei Ueda)

TEL: +81-774-38-4092

FAX: +81-774-38-4094

ABSTRACT

For a small-size geotechnical centrifuge, it is well known that a uniform gravity field, which is position-independent, cannot be achieved in a model ground due to finite lengths of rotating radius: a gravity field in the centrifuge becomes radial. However, little works have been done related to the radial gravity effect on seismic responses of the model ground. This paper presents finite element simulation results for dynamic centrifuge model tests of a liquefiable sloping ground conducted at two centrifuge facilities having different small-radial arms with the shaking direction being tangential to the axis, aiming to show the importance of considering the radial gravity effect in numerical simulation. The simulations are performed in the centrifuge model scale by using a strain space multiple mechanism model; the radial gravity field is applied to the model ground at the stage of self-weight analyses before seismic response analyses are carried out. Comparison of the simulated seismic response with the centrifuge test results demonstrates that the experimental deformation mode due to lateral spreading during shaking is simulated with higher accuracy, particularly near the side boundaries, by considering the small-radius effect (i.e., the radial gravity field instead of the uniform gravity field) in an appropriate manner.

Keywords: Centrifuge model test, Radial gravity field, Finite element Analysis, Strain space multiple mechanism model, Lateral spreading

1. Introduction

The soil liquefaction has been one of the main research areas of the geotechnical community due to continual observance of the catastrophic failure of structures under the phenomenon of soil liquefaction during the recent earthquakes. Over the last few years, the understanding of the soil liquefaction phenomenon has immensely improved because of centrifuge modeling, where the exact phenomenon can be recreated to get a better understanding and to assess its possible impact on the soil-structure interactions. Availability of the case history databases, laboratory soil test data, and centrifuge test results have motivated researchers for the development of various constitutive models. During the VELACS (Verification of Liquefaction Analysis by Centrifuge Studies) project [1], a necessity was felt to validate the centrifuge test results with the various constitutive models and to study the centrifuge test results among the different facilities. However, some variations in the centrifuge test results were found among the different facilities prompting the researchers to study the possible cause of differences among the centrifuge facilities.

After VELACS, another international joint venture called LEAP (Liquefaction Experiments and Analysis Projects) [2] was proposed. The major objective of LEAP is to evaluate the capabilities of various numerical codes for the liquefaction phenomenon using Ottawa F-65 sand as the standard sand for this project. On the sideline of LEAP Project (LEAP GWU-2015), a study was carried out by Tobita et al. [3] to consider the curving effect of the ground surface in centrifuge modeling. The major goal of this research was to study the effect of the radial gravity field for a small size centrifuge that might influence overall results to a large extent.

The difference between the uniform gravity field and non-uniform gravity field has already been studied. The gravity field varies linearly with radius from the center of rotation, r, and as a square of the angular velocity, ω, of the centrifuge, and is explained as $r\omega^2$ [4]. In the radial gravity field, the centrifugal acceleration field that provides the high g is radial by definition emanating outward from the center of rotation of the centrifuge. For both the model and the prototype scale, the total pressure is zero on the surface but is different below the surface, depending on the depth [5].

When geotechnical researchers/engineers try to numerically simulate the experimental results under seismic loading obtained at a small radius centrifuge, it may be necessary to pay attention to the non-uniform gravity field. This is because the seismic response is more or less influenced by the initial stress condition before shaking, which changes depending on the gravity field. However, the influence has not yet been studied in a quantitative way, except for the experimental study by Tobita et al. [3], to the best of authors' knowledge. In particular, no or little consideration has been given to the influence of a small rotation radius when numerical modelers try to simulate centrifuge experimental results.

In this paper, an effort has been made to study the effect of the radial gravity field by carrying out a numerical study using a strain space multiple mechanism model based on finite strain theory incorporating a new stress-dilatancy relationship. Initially, the constitutive model parameters were determined based on the results of cyclic torsional shear tests followed by the numerical analysis of a liquefiable sloping ground. The radial gravity field was applied as body forces in both the vertical and horizontal directions to the model ground at the stage of self-weight analyses before seismic response analyses were carried out.

2. Modeling of a non-uniform gravity field

The radial gravity field in a large radius and a small radius centrifuge for a planar surface model is described in Fig. 1. When the arm length of the centrifuge is large (e.g., the 9 m radius centrifuge at the University of California, Davis), the variation of the centrifugal acceleration on the surface would be small and hence could be ignored. However, this error cannot be ignored for a short radius centrifuge (e.g., the 2.5 m radius centrifuge at the DPRI, Kyoto University): the planar surface of the model may act like a curved surface in prototype scale because centrifugal accelerations applied on the model surface vary depending on the distance between the rotation center and the ground surface.

As shown in Fig. 1, for a larger radius centrifuge, the gravity acts in the nearly vertical direction and does not depend on the depth y; this is because y is negligibly small compared to the large radius r, and thus the angle θ is close to zero (i.e., $r' = r$). Hereafter, this condition is called the "uniform gravity field." On the other hand, the gravity for a smaller radius centrifuge acts in the radial direction due to non-zero θ values and hence the gravity field becomes non-uniform. In this case, the gravity force varies depending on the depth y as well as its horizontal variation described earlier; this is because a change in y cannot be ignored compared to the short radius r. The initial conditions of vertical and horizontal stresses in the model ground before shaking may be influenced by the radial gravity field on a large scale for a small arm centrifuge, which might be critical while studying the subsequent dynamic problems (e.g., liquefaction-induced lateral spreading).

In this study, three different gravity fields are considered, as shown in Table 1 and Fig. 2. Case 1 is an idealized model corresponding to a centrifuge having an infinite length of rotational radius; the direction of gravity acceleration is vertical, and the uniform gravity field can be achieved. However, the gravity field in a short-radius centrifuge becomes non-uniform due to the influence of radial gravity acceleration (Case 2a); in addition, the applied gravity in the ground varies depending on the depth as explained in Fig. 1(b). The third case (i.e., Case 2b) is an imaginary (or unreal) condition: the gravity force in the ground depends on the depth due to a short rotation radius, but the horizontal component of gravity force is ignored (i.e., the gravity direction is assumed vertical).

In the numerical simulation, the radial gravity body forces are applied both in the vertical and horizontal directions for all finite elements during a self-weight analysis prior to shaking events, as described later in subsection 3.3. In this way, the effect of the radial gravity field is reflected in the initial distribution of vertical stresses, horizontal stresses, and shear stresses, which are explained later in Figs. 10 through 12 and in Figs. 17 through 19.

3. Summary of numerical simulation

3.1. Constitutive model

A strain space multiple mechanism model originally proposed by Iai et al. [6] is used for the numerical simulation of the centrifuge experimental tests conducted by Tobita et al. [3, 7]. The model has been extended by incorporating a new stress-dilatancy relationship [8] and implemented in a large deformation analysis program based on the finite strain theory [9]. The analysis program is called "FLIP TULIP" (Finite Element Analysis Program of LIquefaction Process/Total and Updated Lagrangian Program of LIquefaction Process) and is able to consider the geometrical nonlinearity as well as material nonlinearity. The model has been widely used to study the soil-structure interaction problems, including liquefaction under seismic loading, particularly in Japan. A detailed description of the constitutive model can be found in [9, 10].

The numerical simulation results are compared with the centrifuge test results [3, 7] to investigate the effect of the radial gravity field on the seismic response of liquefiable sloping ground in a quantitative way. The centrifuge experiments were conducted at the Disaster Prevention Research Institute, Kyoto University (KyU) using a beam-type centrifuge having an effective radius of 2.5 m as a part of LEAP-GWU-2015 project [2] and at the Center for Geotechnical Modeling at University of California, Davis (UCD) using a beam type centrifuge having an effective radius of 1 m as a part of LEAP-ASIA-2019 [7]. Ottawa F-65 sand was used for both the centrifuge tests. The centrifuge test at KyU was carried out at a relative density of 65%, whereas the centrifuge test at UCD was carried out at a relative density of 67%. The influence of the radial gravity field on the soil model response involving a lateral spreading event is studied by carrying out numerical simulation for the two centrifuge facilities having a different radius of rotation. As shown in Fig. 3, the ground surface is shaped as a curved for both the centrifuge tests to consider the effect of the radial gravity field considering the shaking direction in the plane of spinning of the centrifuge. More detailed information about the centrifuge test method and the test results can be found in [3, 7].

3.2. Determination of model parameters based on Torsional shear test

This subsection explains the selection and determination of constitutive model parameters. The parameters are divided into three types according to the volumetric mechanism, shear mechanism, and dilatancy.

The model parameters were adjusted based on the results of cyclic torsional shear tests for Ottawa F65 Sand carried out by Uemura et al. [11]. The cyclic torsional shear tests were carried out at a relative density of 60% under a confining pressure of 100 kPa. A detailed description of the determination of model parameters can be found in [12]. Tables 2 and 3 represent the model parameters for deformation characteristics and dilatancy, respectively. One of the model parameters defining deformation mechanism r_K was slightly varied between KyU element simulations and UCD element simulations. This was done to achieve a closer EPWP dissipation response to the measured centrifuge response, as shown later in Fig. 15 and Fig. 21. Apart from it, dilatancy parameters defined in terms of $r_{\varepsilon_d^c}$, r_{ε_d} and c_1 were slightly adjusted in order to improve the quality of numerical simulation for the two centrifuge facilities described later in sections 4 and 5. However, the constitutive model parameters were not changed significantly but with minor changes, as shown in Table 2 and Table 3. Hence, the numerical simulations for the cyclic torsional shear test is only shown for KyU in Figs. 4-6 with the dataset of parameters defined in Tables 2 and 3 for KyU for a cyclic stress ratio of 0.20, 0.18, and 0.15. As seen from Figs. 4-6, the experimental results are reasonably simulated for all the cyclic stress ratio values. The increase in strain amplitude, response in terms of stress path, the stress-strain behavior, and the excess pore water pressure (EPWP) generation are found to be well simulated using the constitutive model parameters. Fig. 7 shows the computed liquefaction resistance curves for KyU and UCD with the set of parameters defined in Table 2 and Table 3 for KyU and UCD, respectively. The slight changes made to the constitutive model parameters are found to have minimum influence on the liquefaction resistance curves, and the simulated liquefaction resistance curves for both the facilities for different levels of strain are in good agreement with the torsional shear test results, suggesting that the onset of liquefaction is reasonably represented.

3.3. Analytical conditions

The finite element (FE) analysis was carried out under a two-dimensional plane strain condition. In the numerical simulation, 4-node quadrilateral elements were used along with the reduced integration (SRI) technique [13]. The finite element mesh in Fig. 8 consists of 1701 nodes and 3200 elements, including pore water elements. The element sizes are about one-tenth of the wavelength corresponding to the highest frequency of interest [14].

The degrees of freedom of displacement was fixed at the base in both the lateral and vertical directions, while only lateral displacements were fixed at the side boundaries.

The side and bottom boundaries were set to be impermeable. Pore water pressure boundary was specified to represent a hydrostatic condition along the curved surface. The measured acceleration at the bottom of the rigid box in the centrifuge model test was applied to the base nodes as an input motion (Fig. 9). In both cases, the ramped sinusoidal waves compose 1Hz and 16 cycles and have a peak ground acceleration of 0.15 g.

A self-weight analysis was carried out prior to a dynamic response analysis for evaluating initial stress distribution in the model, where non-uniform gravity force was applied in Case 2a and Case 2b in order to consider its influence on the initial vertical, horizontal and shear stress distribution. In Case 1, the uniform gravity field was applied in a conventional manner.

The numerical time integration for the dynamic response analysis was carried out by the SSpj method [15]. The standard parameters for the SSpj method, i.e., $\theta_1 = 0.6$, $\theta_2 = 0.605$ for the equation of motion and $\theta_1 = 0.6$ for the mass balance equation of pore water flow, were used with a time step of 0.0000225 s in model scale. Rayleigh damping with $\alpha = 0.0$ and $\beta = 0.001$ (or stiffness proportional damping in this case) was used to ensure the stability of the numerical solution process.

4. The numerical simulation results for KyU Centrifuge (Radius = 2.5m) – LEAP-GWU-2015

4.1. Results of self-weight analysis in Case 1, Case 2a and Case 2b

The computed deformed configuration with lateral stress distribution for all the cases is shown in Fig. 10. For Case 1 and Case 2b, the lateral stress is found to be uniformly distributed for a certain depth interval, whereas for Case 2a, the lateral stress is more radially distributed around the radius and its uniformity for the different depth intervals is slightly lesser as compared to Case 1 and Case 2b.

Computed deformed configuration with vertical effective stress is shown in Fig. 11. The variation of the vertical stress with the depth intervals for all the three cases seems to be similar.

Computed deformed configuration with shear stress distribution is shown in Fig. 12. For Case 1 and Case 2b, the concentration zone of shear stresses is found to be present at the bottom of both sides of the soil model. The shear stress zone was induced by applying the vertical gravity, which makes the computed shear stress distribution within the soil model to be completely different from that in Case 2a, where the shear stress is more uniformly distributed throughout the depth by applying the radial field gravity.

4.2. Simulated dynamic response for lateral displacement

Fig. 13(a) represents the simulated lateral displacement response for Case 1. The lateral displacement at the ground surface is underestimated near the right boundary (at *x* = 3*B*/4), while the experimental result for the left part (at *x* = *B*/4) seems to be well simulated, resulting in the same residual lateral displacement towards the end of shaking. At the center part (i.e., *x* = *B*/2), the simulated lateral displacement is found to be less than the measured response, with less values of maximum and residual lateral displacement being computed. It is noted that the measured displacement near the right-side boundary shows a positive directional response, whereas a negative displacement response is obtained from the numerical simulation showing dissimilarity in the deformation modes.

Fig. 13(b) represents the simulated lateral displacement response for Case 2a. The simulated lateral displacement responses at the ground surface are similar to the centrifuge test results at all three locations, with nearly the same residual lateral displacement observed at the end of shaking. This similarity between the centrifuge and simulated response is because of the consideration of the radial gravity field in the numerical model as well as in the centrifuge model.

Fig. 13(c) represents the simulated lateral displacement response for Case 2b. The simulated lateral displacement near the left side boundary (at *x* = *B*/4) is found to be similar to the centrifuge result. However, the measured maximum and residual lateral displacements at the center of the model (*x* = *B*/2) are underestimated by the simulation. In addition, the centrifuge shows a positive lateral displacement near the right-side boundary (at *x* = 3*B*/4), while a negative lateral displacement response is obtained from the simulation showing a difference in the deformation modes. The lateral displacement response for this case is much similar to Case 1 in Fig. 13(a) but different from Case 2a in Fig. 13(b). This means that the influence of depth-dependency in the vertical gravity force (i.e., the difference in the vertical stress distribution between Cases 1 and Case 2b in Fig. 2) is trivial, but the difference between the radial and vertical gravity fields has a great influence on the dynamic response.

4.3. Simulated dynamic response for vertical displacement

The vertical displacement responses are shown in Fig. 14, which is found to be nearly similar between the numerical model and the centrifuge test at all the three locations for Case 1, Case 2a, and Case 2b. Comparison among Case 1, Case 2a, and Case 2b indicates that the difference in the applied gravity fields has no significant effect on the vertical displacement.

4.4. Simulated dynamic response for EPWP

Fig. 15(a) represents the simulated EPWP response for Case 1. The simulated EPWPs in Fig. 15(a) are found to be less than the measured responses throughout the depth at the center ($x = B/2$) of the model. This underprediction of EPWP throughout the depth may lead to an insecure or unsafe design of the soil-structure system against soil liquefaction. However, the maximum EPWP is found to occur at the same duration of loading with nearly similar dissipation responses for the centrifuge and numerical model.

Fig. 15(b) shows the simulated EPWP response for Case 2a. Comparison of Fig. 15(b) with Fig. 15(a) indicates that much better representation of the measured EPWP response is obtained for Case 2a, with nearly similar EPWP generation and dissipation responses at P1 and P2. Towards the ground surface, even Case 2a has yet to fully replicate the experimental results at P3 and P4; however, we tried to do no further recalibration of the model parameters because our primary purpose is to demonstrate the influence of radial gravity fields on the simulated seismic response of a liquefiable sloping ground.

Fig. 15(c) shows the simulated EPWP response for Case 2b, having the same radial distance as that of Case 2a but under the influence of vertical radial gravity field ignoring the horizontal component of the non-uniform centrifugal acceleration. The peak of computed EPWP at P1 for this case is less than the measured response. It is also found to be slightly less than the computed EPWP at P1 for Case 2a shown in Fig. 15(b). However, the computed EPWP response towards the ground surface (P2, P3, and P4) is found to be similar to what was obtained in Case 2a when considering the horizontal component of the radial gravity field in addition to the vertical one (see Fig. 2). Hence, it can be said that the presence or absence of the horizontal gravity component seems to have little influence on the EPWP response near the centerline.

For comparison of the simulated acceleration responses with the measured ones for

Case 1, Case 2a and Case 2b, refer to Fig. A1 in Appendix.

4.5. Comparison among simulated response in Case 1, Case 2a and Case 2b

From the comparison among three cases, it can be said that the seismic responses obtained from Case 2a are found to be in good agreement with the centrifuge test results, particularly in terms of lateral displacements and EPWP. On the other hand, the centrifuge test results (particularly in terms of lateral displacement responses of the soil model) cannot be reasonably simulated in Case 1, which does not consider the radial gravity field effect, and in Case 2b, which only considers the depth-dependency of vertical gravity force. Hence, consideration of the effect of the radial gravity field would be a critical step for the numerical modelers in order to predict the soil response more accurately.

4.6. The deformation with excess pore water pressure ratio

Computed deformed configurations with the distribution of EPWP ratio for Case 1, Case 2a, and Case 2b are shown in Fig. 16. The snapshots were taken at around 12 seconds when the lateral displacement at the center of the ground surface was computed to be maximum for all three cases. Although the EPWP ratio response in the center of the soil model is found to be comparable among the cases, Case 2a predicts the occurrence of soil liquefaction throughout the depth of soil model near the centerline.

The EPWP obtained for Case 2a at P1 near the bottom of the centerline (see Fig. 3) was found to be larger than that in Case 1 and Case 2b, whose EPWP response was found to be similar, thus validating the EPWP ratio variation near the centerline towards the bottom of soil model observed in Fig. 16. The distribution near the two sides of the soil model in Case 2a also shows higher EPWP values, predicting the occurrence of soil liquefaction, and differs significantly from the lower EPWP values in Case 1 and Case 2b; this difference is considered to be reflected in the simulated response of lateral displacements particularly near the right side boundary as described in subsection 4.2. As well as the similarity in the simulated lateral displacement responses between Case 1 in Fig. 13(a) and Case 2b in Fig. 13(c), similar EPWP distributions (i.e., localized EPWP increase near the center zone) are obtained for the two cases, as shown in Figs. 16(a) and 16(c).

Hence, it can be said that the presence or absence of the horizontal gravity component arising from the radial gravity field (see Fig. 2) has a significant impact on the distribution of the EPWP ratio, particularly near the side boundaries. On the other hand, only taking into account the depth-dependency of vertical gravity force is found not to greatly affect the EPWP distribution from a comparison between Figs. 16(a) and 16(c).

5. The numerical simulation results for UCD Centrifuge (Radius = 1.0m) – LEAP-ASIA-2019

5.1. Results of self-weight analysis in Case 1, Case 2a and Case 2b

The computed deformed configuration with lateral stress for all the cases is shown in Fig. 17. The lateral stress for Case 2a is found to be radially distributed towards the side boundaries, whereas for Case 1 and Case 2b, the lateral stress is found to be uniformly distributed for a certain depth interval. This distribution of lateral stress is similar to the computed deformed configuration for KyU shown in Fig. 10.

The distribution of computed vertical effective stress is shown in Fig. 18. The variation of the vertical stress is observed to be similar for all the cases throughout the entire width and depth of the soil model.

The distribution of computed shear stress is shown in Fig. 19. A similar shear stress distribution is observed between Case 1 and Case 2b with a concentration zone of shear stress found to be present near the left side boundary at the bottom of the soil model. However, the shear stress distribution in Case 2a is significantly different from that in Case 1 and Case 2b: the presence of the horizontal gravity component (see Fig. 2) leads to the right and left reversed sign of shear stress near the bottom in Fig. 19(b) opposite to Figs. 19(a) and 19(c).

5.2. Simulated dynamic response for lateral displacement

Fig. 20(a) shows the simulated lateral displacement response for Case 1, which represents the infinite radius condition simulating a large radius centrifuge. The simulated lateral displacement at the ground surface is found to be similar to the measured one near the left side boundary (x = B/4). However, the simulation slightly underestimates the measured lateral displacement at the center of the model (x = B/2). Near the right-side boundary (x = 3B/4), the measured displacement increases in the positive direction towards its residual value, while the lateral displacement in the opposite direction is obtained from the numerical simulation.

Fig. 20(b) indicates the simulated lateral displacement response for Case 2a, which represents the UCD Centrifuge having an effective radius of 1 m considering the influence of the radial gravity field. As shown in Fig. 20(b), slight differences are observed near the left side boundary (x = B/4) and at the center of soil model (x = B/2) as compared to the measured centrifuge response. On the other hand, the simulated lateral displacement near the right side boundary (x = 3B/4) is found to be close to the centrifuge test with nearly identical residual displacements. Despite the differences at x = B/4, and B/2, the overall deformation mode observed in the centrifuge is considered to be well reproduced in the simulation compared to the simulated results in Case 1 (see Fig. 20(a)).

Fig. 20(c) represents the simulated lateral displacement response for Case 2b, which has the same radius distance as of Case 2a but under the influence of only the non-uniform vertical gravity field. The simulated lateral displacement near the left side boundary ($x = B/4$) is found to be in close agreement with the centrifuge result. However, the simulation slightly underestimates the measured lateral displacement at the center of the model ($x = B/2$) with disagreement in the residual lateral displacement. Near the right-side boundary ($x = 3B/4$), the simulated and measured lateral displacements are observed to have differences in the deformation mode.

5.3. Simulated dynamic response for EPWP

The simulated EPWP responses are nearly similar to the centrifuge results as shown in Fig. 21 for Case 1, Case 2a, and Case 2b. However, the dissipation speed of simulated EPWP is found to be slightly different from the centrifuge test throughout the depth of soil model for Case 1, whereas it is found to be much closer to the centrifuge test for Case 2a. For Case 2b, the rate of dissipation of simulated EPWP is found to be slightly different from the centrifuge test, with much rapid dissipation being observed in the measured response, particularly at P1 and P2.

For the simulated acceleration responses for Case 1, Case 2a and Case 2b, see Fig. A2 in Appendix.

5.4. Comparison among simulated response in Case 1, Case 2a and Case 2b

From the above three cases for a centrifuge having a much smaller radial arm (UCD, radius = 1.0 m), it can be said Case 2a response is a much better representation of the centrifuge result as compared to Case 1 and Case 2b. The lateral displacement response is extremely critical when dealing with the lateral spreading of soil layers during a seismic event (particularly for soil-structure interactions), and hence it becomes essential for the numerical modelers to achieve accurate results, which may simulate centrifuge test response qualitatively. The consideration of the radial gravity field may be an ideal option for such scenarios, especially when simulating the response of centrifuge having a small radius. The lateral displacement responses for Case 1, where the gravity field was assumed uniform, and for Case 2b, where the horizontal component of the radial gravity field was ignored, are found to be significantly different from the centrifuge response. The estimated lateral displacement responses for Case 1, Case 2a, and Case 2b may have been influenced by the distribution of initial shear stress following the self-weight analysis shown in Fig. 19. For Case 2a, positive shear stress is induced on the right side of the soil model, while for Case 1 and Case 2b, negative shear stress is found to occur on the right side of the model and similar changes in deformation modes are observed for Case 1 and Case 2b, with the occurrence of negative lateral displacement on the right side of the model opposite to Case 2a and the measured centrifuge response. The rate of dissipation of EPWP for Case 2a is also found to be much closer to the centrifuge response as compared to Case1 and Case 2b.

5.5. The deformation with excess pore water pressure ratio

The deformed mesh with the variation of EPWP ratio throughout the depth of the soil model for Case 1, Case 2a, and Case 2b is shown in Fig. 22. The deformed mesh represents the EPWP ratio at around 12 seconds when the lateral displacement is computed to be maximum for all the three cases. The deformed mesh is much similar to the mesh obtained for KyU, as shown in Fig. 16. The EPWP ratio variation is found to be similar for Case 1 and Case 2b, while a significantly different response is observed for Case 2a. The soil is found to liquefy near the center zone of the soil model for all the cases throughout the depth. However, Case 2a predicts the occurrence of soil liquefaction near the side boundaries as well for a certain depth. The response for Case 1 and Case 2b is in close agreement to the numerically simulated response for the lateral displacement, as shown in Fig. 20(a) and 20(c), where significantly different values of lateral displacement are recorded at (x = 3B/4) near the ground surface as compared to Case 2a. The consideration of the radial gravity field may lead to a much safer analysis taking into account the widespread occurrence of soil liquefaction, which is represented in Case 2a.

6. Conclusions

This paper presents the numerical simulation results for dynamic centrifuge tests for a liquefiable sloping ground carried out at two different centrifuge facilities having a different radial arm of rotation, focusing on the influence of the radial gravity field in a short-radius centrifuge involving shaking perpendicular to the axis. The simulations were conducted using a strain space multiple mechanism model based on the finite strain theory. At a self-weight analysis prior to a seismic response analysis, three different gravity fields were applied: 1) uniform vertical gravity force, which is position-independent and corresponds to an infinite length of rotation radius (Case 1), 2) non-uniform radial gravity force, which varies depending on both horizontal and vertical positions corresponding to a short rotation radius (Case 2a), 3) non-uniform vertical gravity force, which only depends on depth even though the length of rotation radius is the same as Case 2a (Case 2b).

Following conclusions are derived from this study:

- After the self-weight analysis (for both KyU and UCD), the computed lateral stress in Case 2a was found to be radially distributed towards the side boundaries, whereas the lateral stress in Case 1 and Case 2b was more uniformly distributed for a certain depth interval. The vertical stress distribution was almost similar among the three cases. When it comes to the shear stress distribution, Case 2a was significantly different from Case 1 and Case 2b; in the latter two cases, the region of shear stress concentration was observed near the bottom of the ground.
- The variations observed in shear stress distributions may have led to significantly different lateral displacement responses (or deformation modes) under seismic

loading among the cases: the simulated response in Case 2a was nearly similar to the centrifuge experimental response (for both KyU and UCD), whereas the results in Case 1 and Case 2b differed significantly from the experiments particularly near the side boundaries. Hence, it can be said that Case 2a was able to simulate the measured lateral displacements and deformation mode with a high degree of accuracy by considering the radial gravity field effect with the correct distribution of initial shear stress following the self-weight analysis. It is also interesting to note the less variations in the shear stress distribution obtained for KyU as compared to UCD centrifuge. This may possibly be due to the lesser influence of the radial field gravity for a centrifuge having a larger radius.

- The simulated lateral displacements in Case 2b were much similar to those in Case 1 but significantly different from those in Case 2a, particularly near the side boundaries. This demonstrates that the influence of depth-dependency in the vertical gravity force (i.e., the difference in the vertical stress distribution between Cases 1 and 2b) is trivial, but the difference between the radial and vertical gravity fields has a great influence on the dynamic response.
- The simulated lateral displacement responses for both the centrifuge facilities were found to be nearly similar among the cases near the centerline of the soil model. This indicates that the presence or absence of the horizontal component of radial gravity field (for Case 2a and Case 2b, respectively) has a little influence on the

center region of the soil system, as well as a slight impact of the depth-dependency in the vertical gravity force (from a comparison between Case 1 and Case 2b).

- The simulated EPWP distribution near the side boundaries in Case 2a was significantly different from that in Case 1 and Case 2b; Case 2a indicated the occurrence of liquefaction near the sides, while Case 1 and Case 2b predicted the soil system response to be safer against soil liquefaction. This difference is thought to be the cause of the aforementioned difference in lateral displacements near the side boundaries between Case 2a and the others. Hence, it can be said the radial gravity effect seems to be predominant near the sides of the soil model.

Acknowledgments

The authors are grateful to all the centrifuge facility groups, who took part in the LEAP Project and allowed their data to be used for numerical simulation exercise.

Appendix A

The simulated time histories of horizontal accelerations at the centerline of the soil model are compared with the centrifuge test results in Fig. A1 for KyU and in Fig. A2 for UCD. To summarize the acceleration responses in the figures, no significant effect of the modeling of the gravity field was observed; the experimental results were well simulated in all cases.

References

[1] Arulanandan K, Scott RF. Verification of Numerical Procedures for the Analysis of Soil Liquefaction Problems. Proceedings of the international conference on the Verification of Numerical Procedures for the Analysis of Soil Liquefaction Problems 1993 and 1994;(1-2): A. A. Balkema.

[2] Kutter BL, Carey TJ, Hashimoto T, Zeghal M, Abdoun T, Kokkali P, et al. LEAP-GWU-2015 Experiment Specifications, Results, and Comparisons. Soil Dynamics and Earthquake Engineering 2018; 113: 616-628.

[3] Tobita T, Ashino T, Ren J, Iai S. Kyoto University LEAP-GWU-2015 tests and the importance of curving the ground surface in centrifuge modelling. Soil Dynamics and Earthquake Engineering 2018; 113: 650–662.

[4] Madabhushi, G. Centrifuge Modelling for Civil Engineers. Boca Raton: CRC Press/Taylor & Francis; 2015.

[5] Schofield AN. Cambridge Geotechnical Centrifuge Operations. Geotechnique 1980; 30: 227-8.

[6] Iai S, Matsunaga Y, Kameoka T. Strain space plasticity model for cyclic mobility. Soils and Foundations 1992; 32(2): 1-15.

[7] Tobita T, Vargas RR, Ichii K, Okamura M, Sjafruddin A N, Takemura J, et al. LEAP-ASIA-2018: Validation of centrifuge experiments and generalized scaling law on liquefaction-induced lateral spreading. Forthcoming, Submitted to the Journal of Soil Dynamics and Earthquake Engineering (special issue on LEAP-ASIA 2019).

[8] Iai S, Tobita T, Ozutsumi O, Ueda K. Dilatancy of granular materials in a strain space multiple mechanism model. International Journal for Numerical and Analytical Methods in Geomechanics 2011;35(3):360-2.

[9] Iai S, Ueda K, Tobita T, Ozutsumi O. Finite strain formulation of a strain space multiple mechanism model for granular materials. International Journal for Numerical and Analytical Methods in Geomechanics 2013;37(9):1189-2.

[10]Ueda K. Finite Strain Formulation of a Strain Space Multiple Mechanism Model for Granular Materials and Its Application, Doctoral Thesis, Kyoto University, 2009 (in Japanese).

[11]Uemura K, Vargas R, Ueda K. LEAP-Asia-2018: Stress-strain response of Ottawa sand in Cyclic Torsional Shear Tests, 2018. DesignSafe-CI, https://doi.org/10.17603/DS28D8G.

[12] Ueda K, Iai S. Numerical Predictions for Centrifuge Model Tests of a Liquefiable Sloping Ground Using a Strain Space Multiple Mechanism Model Based on the Finite Strain Theory. Soil Dynamics and Earthquake Engineering 2018; 113: 771–792.

[13]Hughes TJR. Generalization of selective integration procedures to anisotropic and nonlinear media. International Journal for Numerical Methods in Engineering 1980; 15: 1413-8.

[14]Alford RM, Kelly KR, Boore DM. Accuracy of finite difference modeling of the acoustic wace equation. Geophysics 1974; 39(6): 834-2.

[15]Zienkiewicz OC, Taylor RL, Zhu JZ. The Finite Element Method: Its Basis and Fundamentals (sixth edition). Elsevier 2000.

Figure Legends

Fig. 1 The radial gravity field in a large diameter centrifuge and a small diameter centrifuge.

Fig. 2 The gravity field considered for the different cases: (a) Case 1 (b) Case 2a (c) Case 2b.

Fig. 3 Schematic model for LEAP GWU 2015 and LEAP ASIA 2019 centrifuge tests for the curved surface (Kutter et al., 2018).

Fig. 4 Simulation of cyclic undrained torsional shear tests (confining pressure=100 kPa, cyclic ratio=0.20): (a) Effective stress path; (b) Stress vs strain; (c) Time history of Shear strain; (d) Time history of excess pore water pressure ratio.

Fig. 5 Simulation of cyclic undrained torsional shear tests (confining pressure=100 kPa, cyclic ratio=0.18): (a) Effective stress path; (b) Stress vs strain; (c) Time history of Shear strain; (d) Time history of excess pore water pressure ratio.

Fig. 6 Simulation of cyclic undrained torsional shear tests (confining pressure=100 kPa, cyclic ratio=0.15): (a) Effective stress path; (b) Stress vs strain; (c) Time history of Shear strain; (d) Time history of excess pore water pressure ratio.

Fig. 7 Computed liquefaction resistance curves with measured plots: (a) KyU (b) UCD

Fig. 8 Finite element mesh for numerical analysis.

Fig. 9 Input motion (a) KyU Centrifuge (LEAP GWU2015), (b) UCD Centrifuge (LEAP ASIA2019).

Fig. 10 Computed deformed configuration with lateral stress at the end of self-weight analysis: (a) Case 1; (b) Case 2a; (c) Case 2b of KyU (LEAP GWU2015).

Fig. 11 Computed deformed configuration with vertical stress at the end of self-weight analysis: (a) Case 1; (b) Case 2a; (c) Case 2b of KyU (LEAP GWU2015).

Fig. 12 Computed deformed configuration with shear stress at the end of self-weight analysis: (a) Case 1; (b) Case 2a; (c) Case 2b of KyU (LEAP GWU2015).

Fig. 13 Computed time history of lateral displacement for KyU Centrifuge (LEAP GWU-2015): (a) Case 1; (b) Case 2a; (c) Case 2b.

Fig. 14 Computed time history of vertical displacement for KyU Centrifuge (LEAP GWU-2015): (a) Case 1; (b) Case 2a; (c) Case 2b.

Fig. 15 Computed time history of excess pore water pressure for KyU Centrifuge (LEAP GWU-2015): (a) Case 1; (b) Case 2a; (c) Case 2b.

Fig. 16 Computed deformed configuration with excess pore water pressure ratio before the maximum deformation: (a) Case 1; (b) Case 2a; (c) Case 2b for KyU Centrifuge (LEAP GWU-2015).

Fig. 17 Computed deformed configuration with lateral stress at the end of self-weight analysis: (a) Case 1; (b) Case 2a; (c) Case 2b for UCD Centrifuge (LEAP ASIA-2019).

Fig. 18 Computed deformed configuration with vertical stress at the end of self-weight analysis: (a) Case 1; (b) Case 2a; (c) Case 2b for UCD Centrifuge (LEAP ASIA-2019).

Fig. 19 Computed deformed configuration with shear stress at the end of self-weight analysis: (a) Case 1; (b) Case 2a; (c) Case 2b for UCD Centrifuge (LEAP ASIA-2019).

Fig. 20 Computed time history of lateral displacement for UCD Centrifuge (LEAP ASIA-2019): (a) Case 1; (b) Case 2a; (c) Case 2b.

Fig. 21 Computed time history of excess pore water pressure for UCD Centrifuge (LEAP ASIA-2019): (a) Case 1; (b) Case 2a; (c) Case 2b.

Fig. 22 Computed deformed configuration with excess pore water pressure ratio before the maximum deformation: (a) Case 1; (b) Case 2a; (c) Case 2b of UCD (LEAP ASIA-2019).

Fig. A1 Computed time history of horizontal accelerations for KyU Centrifuge (LEAP-GWU-2015): (a) Case 1; (b) Case 2a; (c) Case 2b

Fig. A2 Computed time history of horizontal accelerations for UCD Centrifuge (LEAP ASIA-2019): (a) Case 1; (b) Case 2a; (c) Case 2b

Table Legends

Table 1 Different cases of numerical analysis considered for KyU (LEAP GWU2015) and UCD (LEAP ASIA2019).

Table 2 Model parameters for deformation characteristics.

Table 3 Model parameters for dilatancy.

Table 1 Different cases of numerical analysis considered for: (a) KyU (LEAP GWU2015), (b) UCD (LEAP ASIA2019).

(a)

Case		Effective radius (m)	Gravity field	Gravity direction	Depth dependency
Kyoto University (Tobita et al., 2018)		2.5	Non-uniform	Radial	Yes
Numerical simulation	Case1	∞	Uniform	Vertical	No
	Case2a	2.5	Non-uniform	Radial	Yes
	Case2b	2.5	Non-uniform	Vertical	Yes

(b)

Case		Effective radius (m)	Gravity field	Gravity direction	Depth dependency
UC Davis (Tobita et al., 2020)		1.0	Non-uniform	Radial	Yes
Numerical simulation	Case1	∞	Uniform	Vertical	No
	Case2a	1.0	Non-uniform	Radial	Yes
	Case2b	1.0	Non-uniform	Vertical	Yes

Table 2 Model parameters for deformation characteristics.

Symbol	Parameter designation	KyU	UCD
ρ_t	Mass density (t/m^3)	2.092	2.092
P_a	Reference confining pressure (kPa)	75.0	75.0
$K_{L/Ua}$	Bulk modulus (kPa)	160837	160837
r_K	Reduction factor of bulk modulus for liquefaction analysis	0.65	0.5
l_K	Power index of bulk modulus for liquefaction analysis	2.0	2.0
G_{ma}	Shear modulus (kPa)	61674	61674
ϕ_f^{PS}	Internal friction angle for plane strain(°)	36.6	36.6
h_{max}	Upper bound for hysteretic damping factor	0.24	0.24

Table 3 Model parameters for dilatancy.

Symbol	Parameter designation	KyU	UCD
ϕ_p	Phase transformation angle (°)	28.0	28.0
ε_d^{cm}	Limit of contractive component	0.2	0.2
$r_{\varepsilon_d^c}$	Parameter controlling contractive component	1.0	1.5
r_{ε_d}	Parameter controlling dilative and contractive components	0.8	0.7
q_1	Parameter controlling initial phase of contractive component	8.0	8.0
q_2	Parameter controlling final phase of contractive component	1.0	1.0
S_1	Small positive number to avoid zero confining pressure	0.005	0.005
c_1	Parameter controlling elastic rage for contractive component	1.67	1.69
q_{us}	Undrained shear strength (for steady state analysis)	-	-

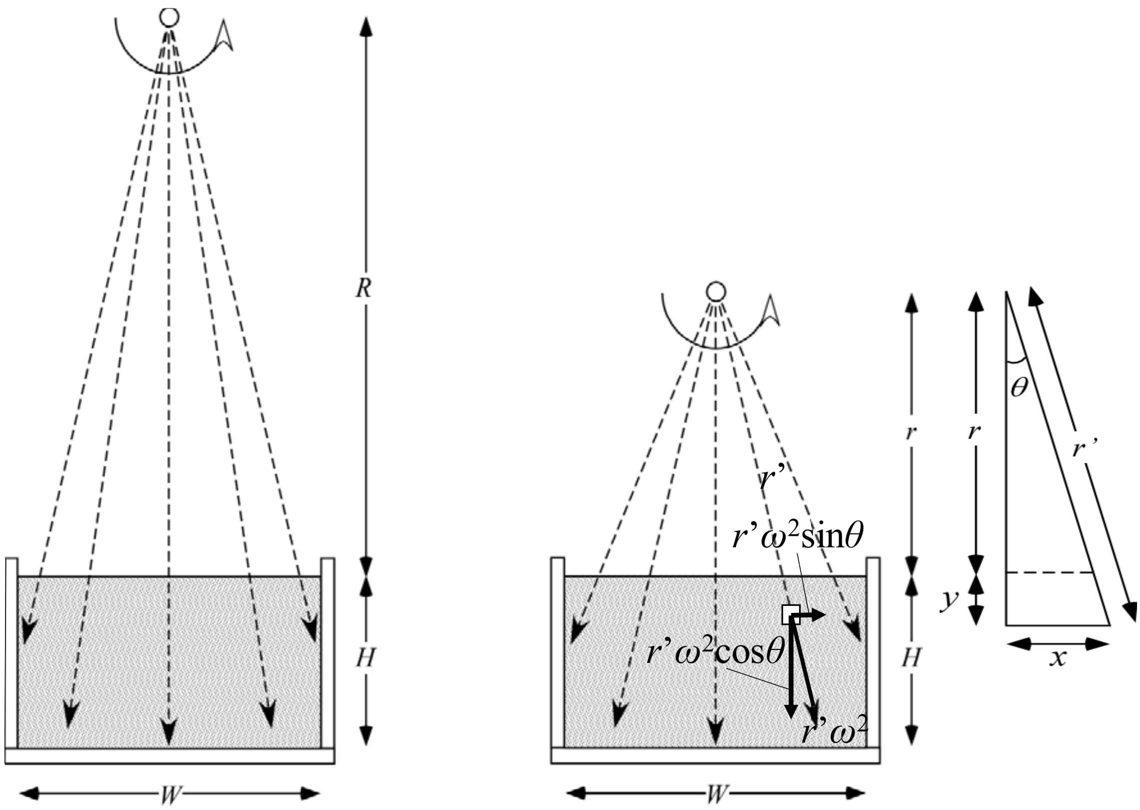

(a) **(b)**

Figure 1 The radial gravity field: (a) in a large-diameter centrifuge (e.g. The 9 m radius centrifuge of the University of California, Davis), (b) in a small-diameter centrifuge (e.g. The 2.5 m radius centrifuge of the DPRI, Kyoto University)

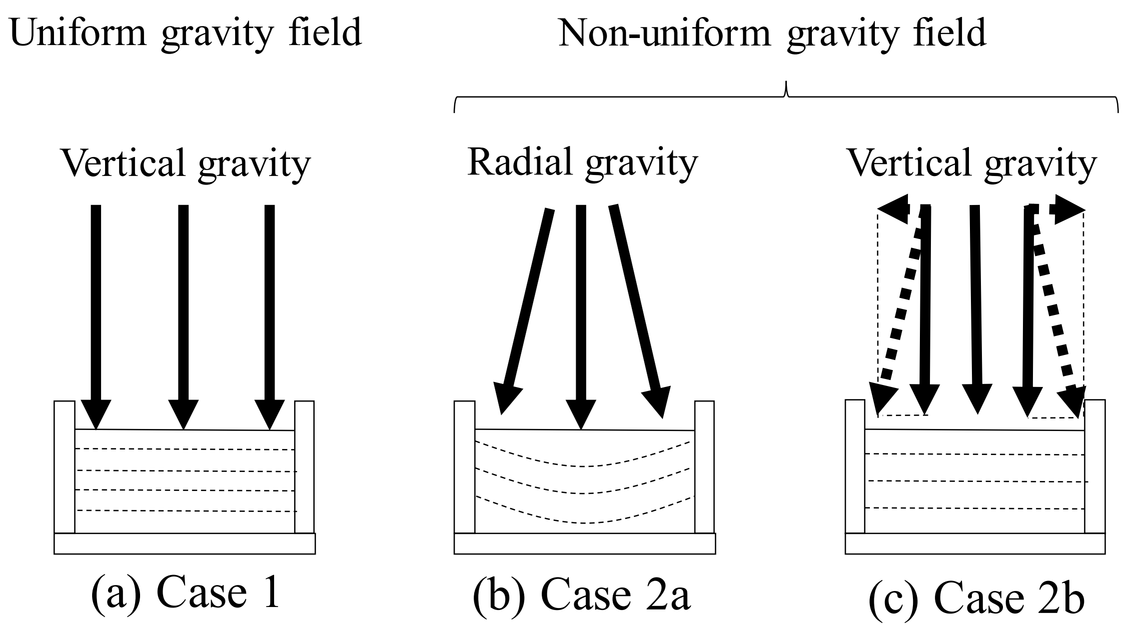

Figure 2 The gravity field considered for the different cases: (a) Case 1, (b) Case 2a, (c) Case 2b

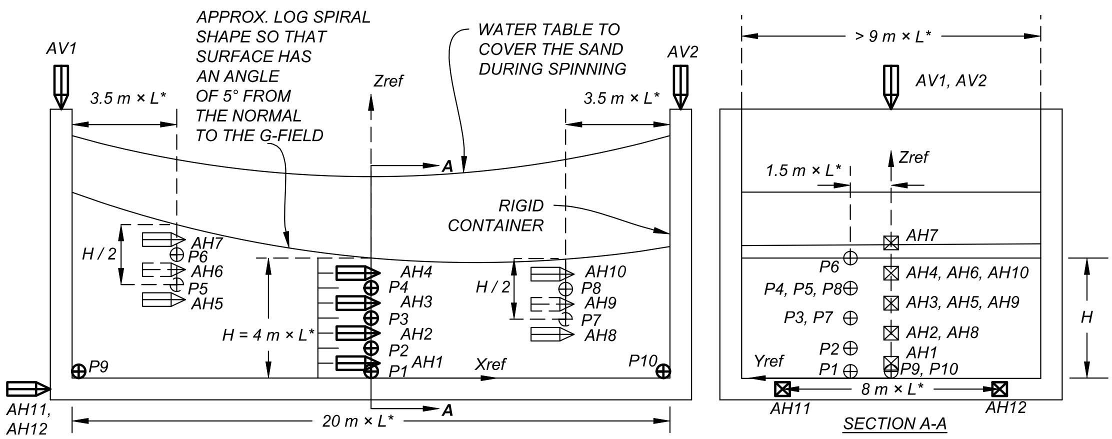

Figure 3 Schematic model for LEAP GWU 2015 and LEAP ASIA 2019 centrifuge tests for the curved surface (Kutter et al., 2018)

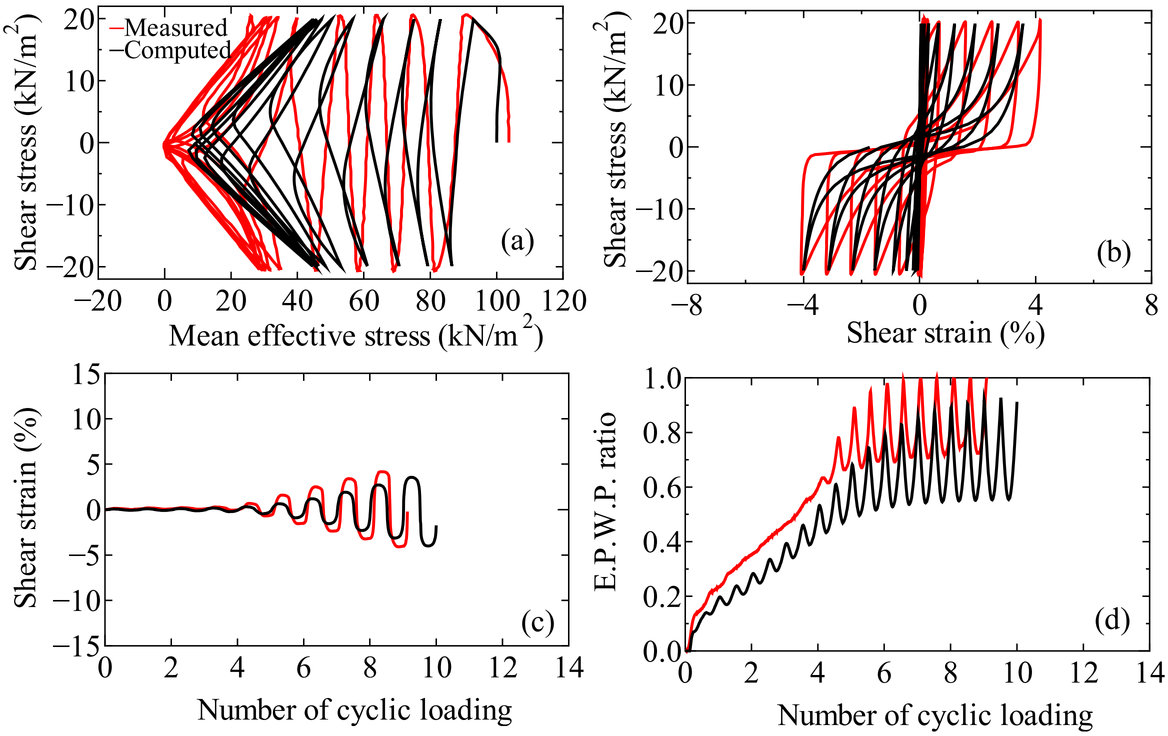

Figure 4 Simulation of cyclic undrained torsional shear tests (confining pressure=100 kPa, cyclic ratio=0.20): (a) Effective stress path; (b) Stress vs strain; (c) Time history of Shear strain; (d) Time history of excess pore water pressure ratio.

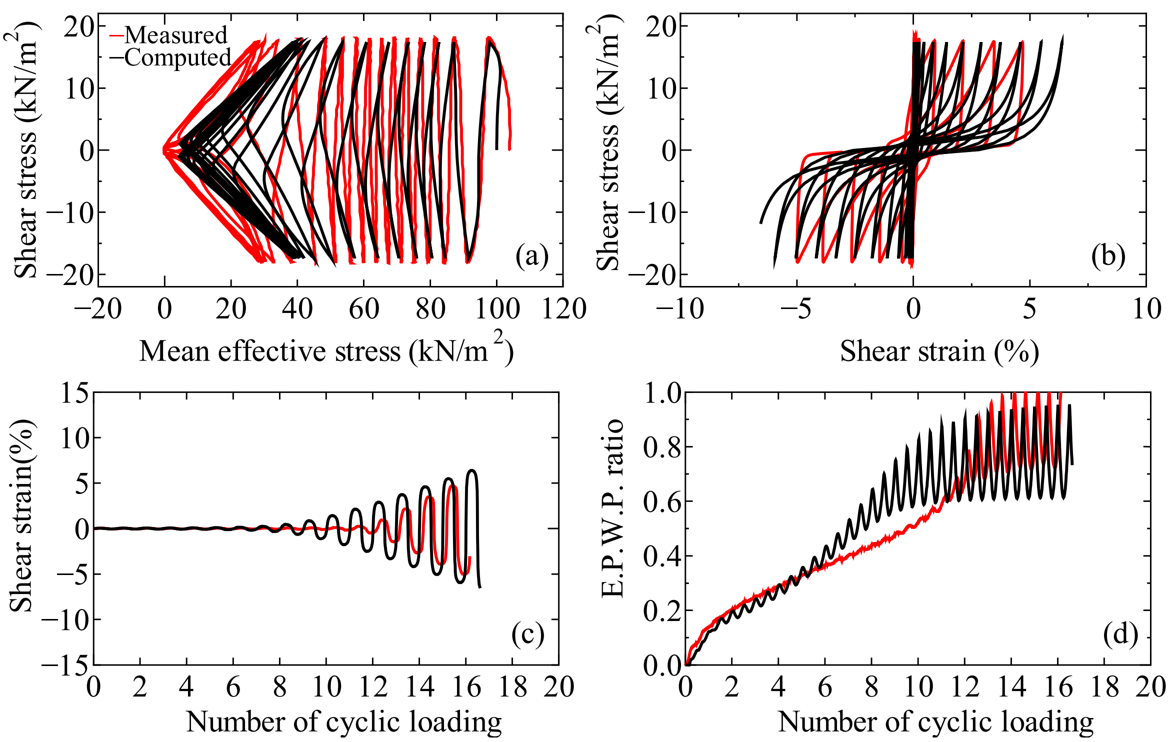

Figure 5 Simulation of cyclic undrained torsional shear tests (confining pressure=100 kPa, cyclic ratio=0.18): (a) Effective stress path; (b) Stress vs strain; (c) Time history of Shear strain; (d) Time history of excess pore water pressure ratio.

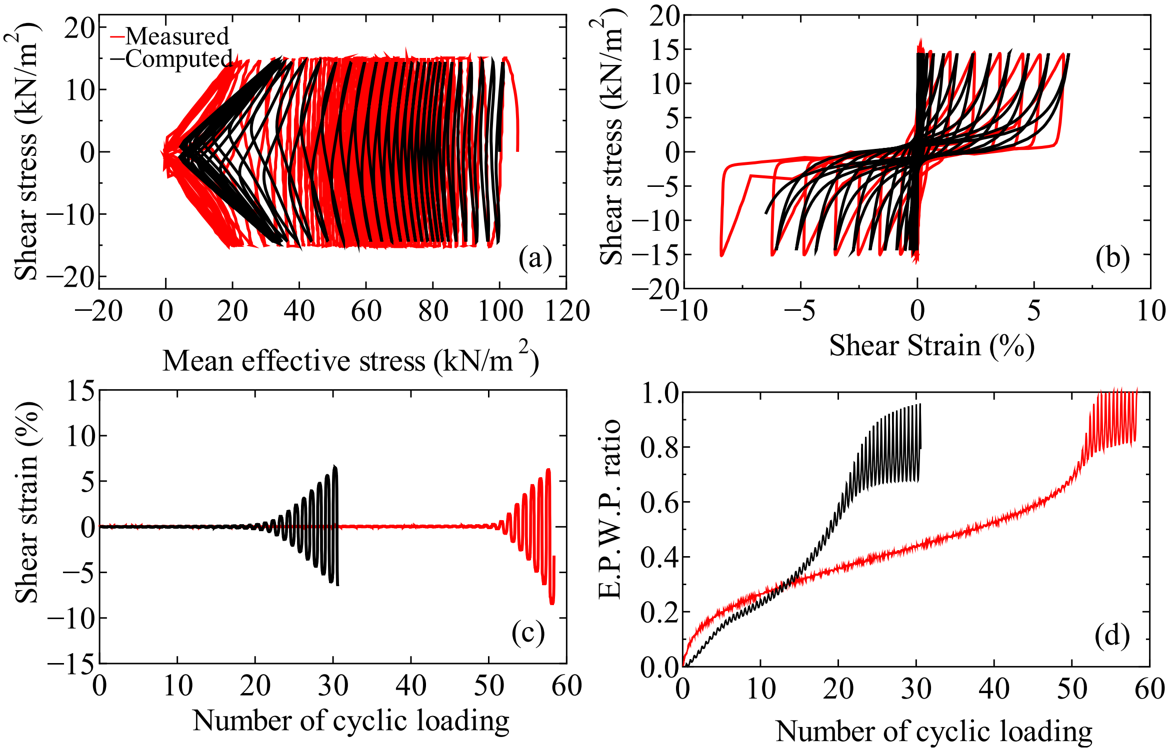

Figure 6 Simulation of cyclic undrained torsional shear tests (confining pressure=100 kPa, cyclic ratio=0.15): (a) Effective stress path; (b) Stress vs strain; (c) Time history of Shear strain; (d) Time history of excess pore water pressure ratio.

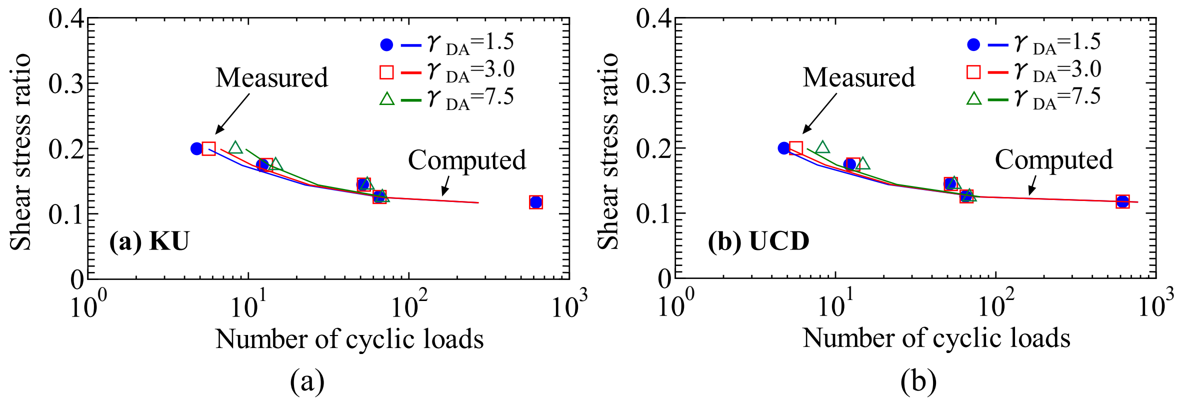

Figure 7 Computed liquefaction resistance curves with measured plots: (a) KyU, (b) UCD

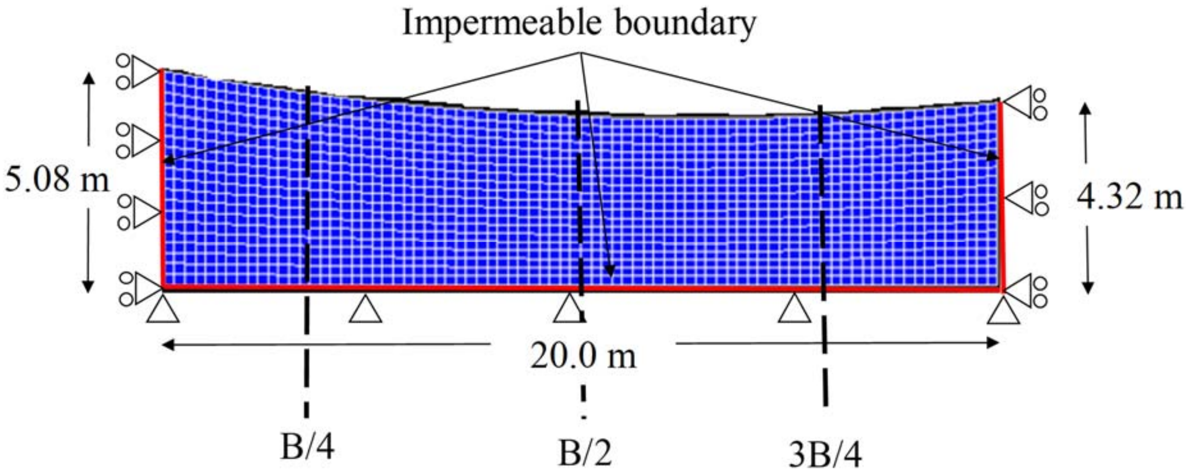

Figure 8 Finite element mesh for numerical analysis

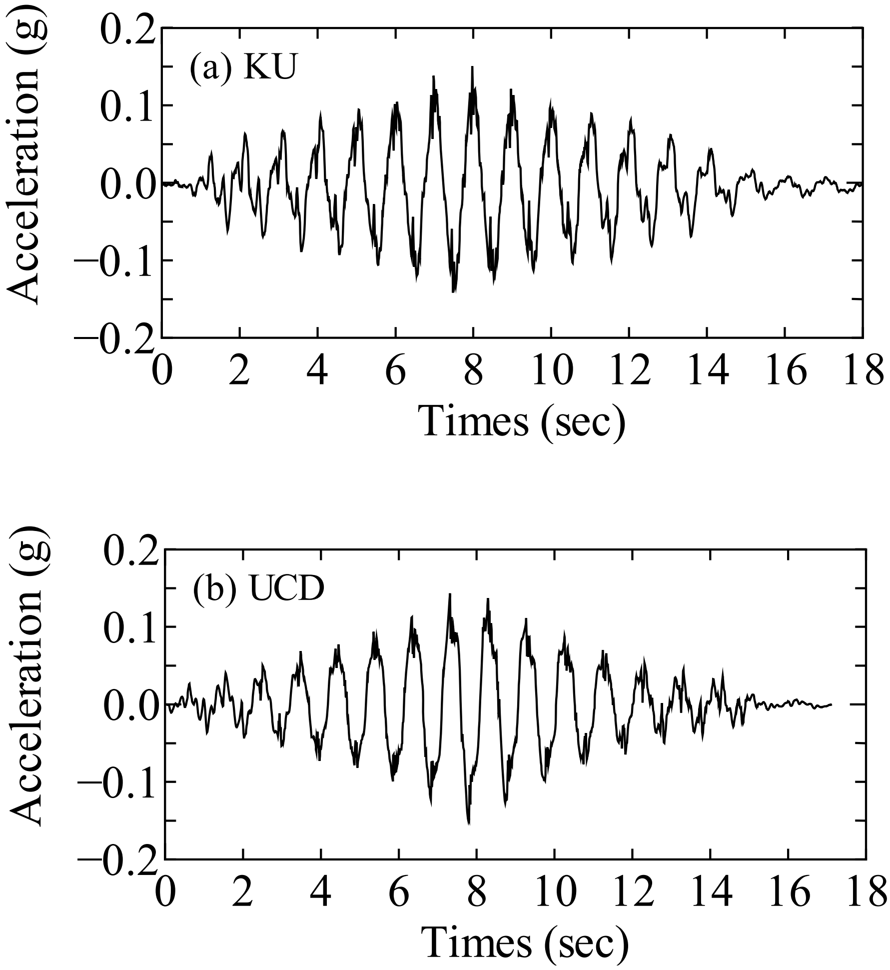

Figure 9 Input motion (a) KyU Centrifuge (LEAP GWU2015), (b) UCD Centrifuge (LEAP ASIA2019)

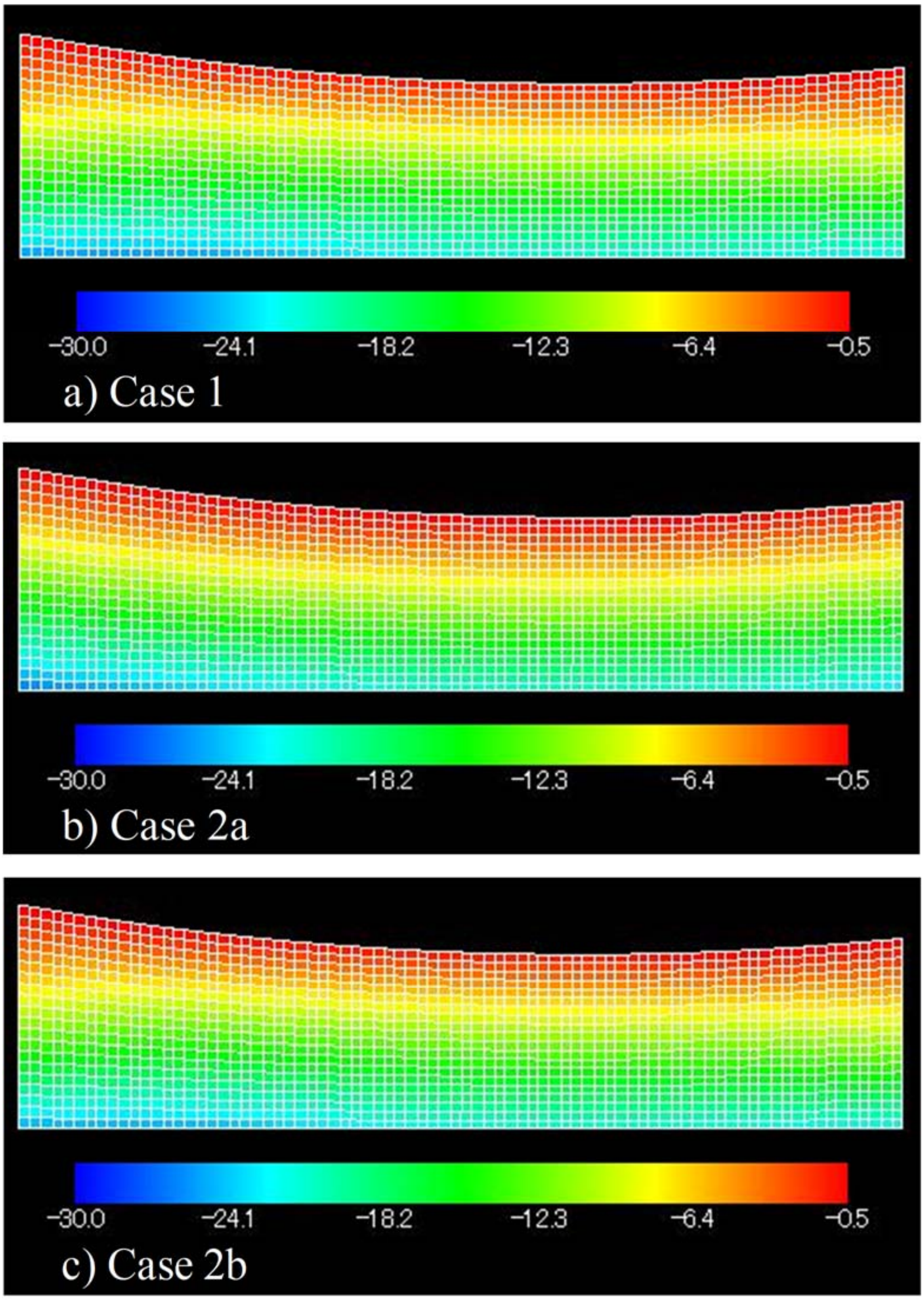

Figure 10 Computed deformed configuration with lateral stress at the end of self-weight analysis: (a) Case 1; (b) Case 2a; (c) Case 2b of KyU Centrifuge (LEAP-GWU-2015)

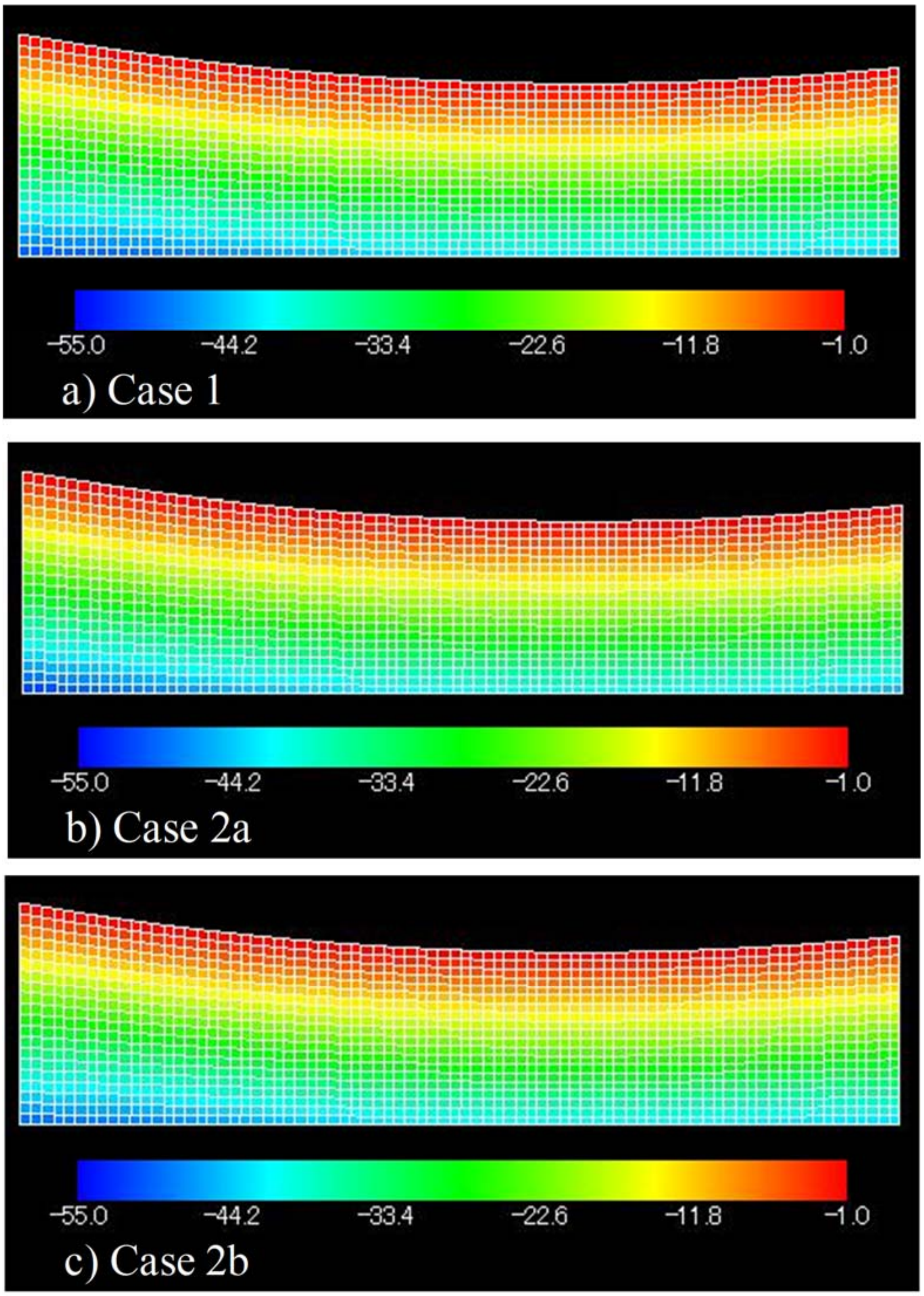

Figure 11 Computed deformed configuration with vertical stress at the end of self-weight analysis: (a) Case 1; (b) Case 2a; (c) Case 2b of KyU Centrifuge (LEAP-GWU-2015).

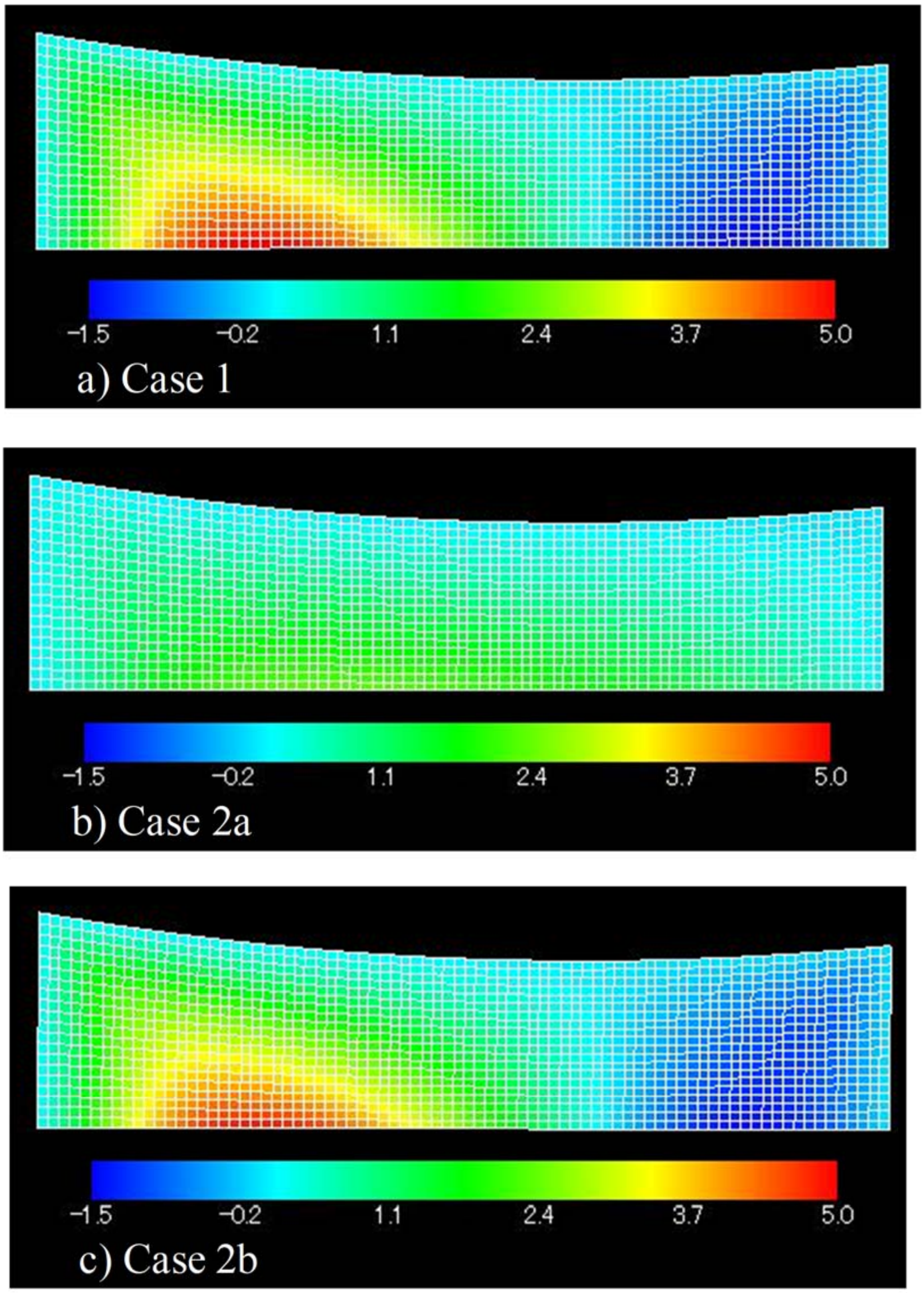

Figure 12 Computed deformed configuration with shear stress at the end of self-weight analysis: (a) Case 1; (b) Case 2a; (c) Case 2b of KyU Centrifuge (LEAP-GWU-2015).

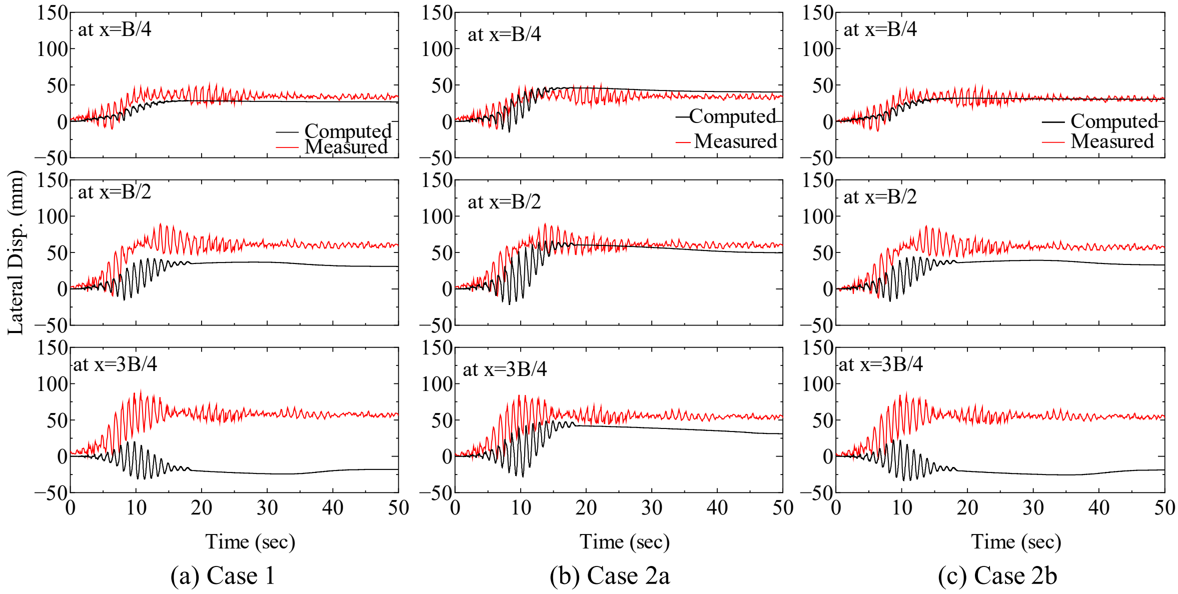

Figure 13 Computed time history of lateral displacement for KyU Centrifuge (LEAP-GWU-2015): (a) Case 1; (b) Case 2a; (c) Case 2b

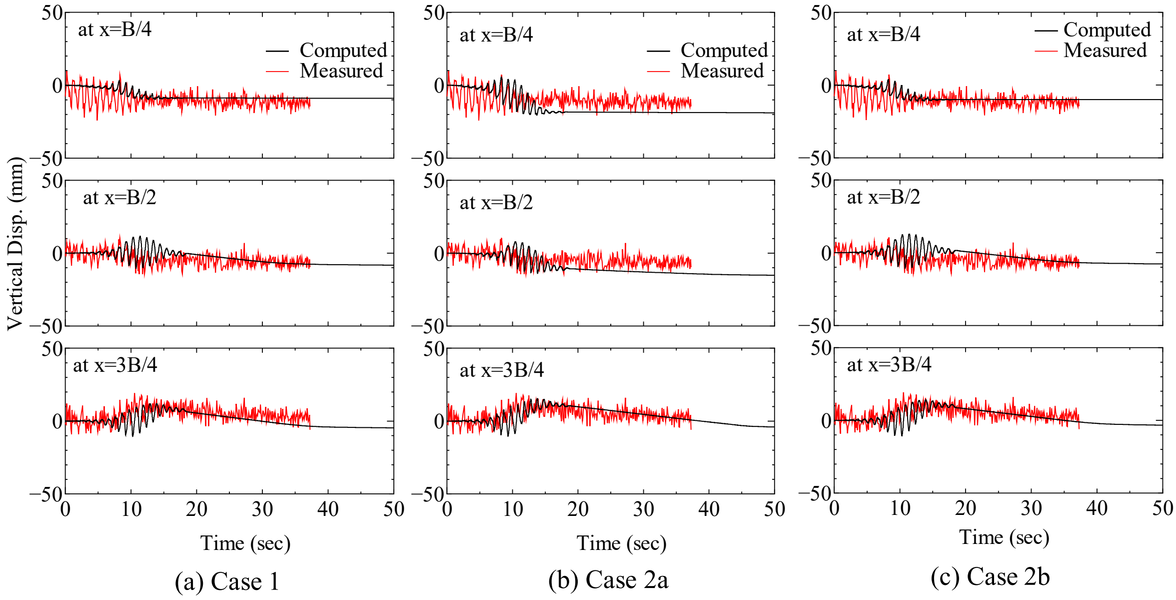

Figure 14 Computed time history of vertical displacement for KyU Centrifuge (LEAP-GWU-2015): (a) Case 1; (b) Case 2a; (c) Case 2b

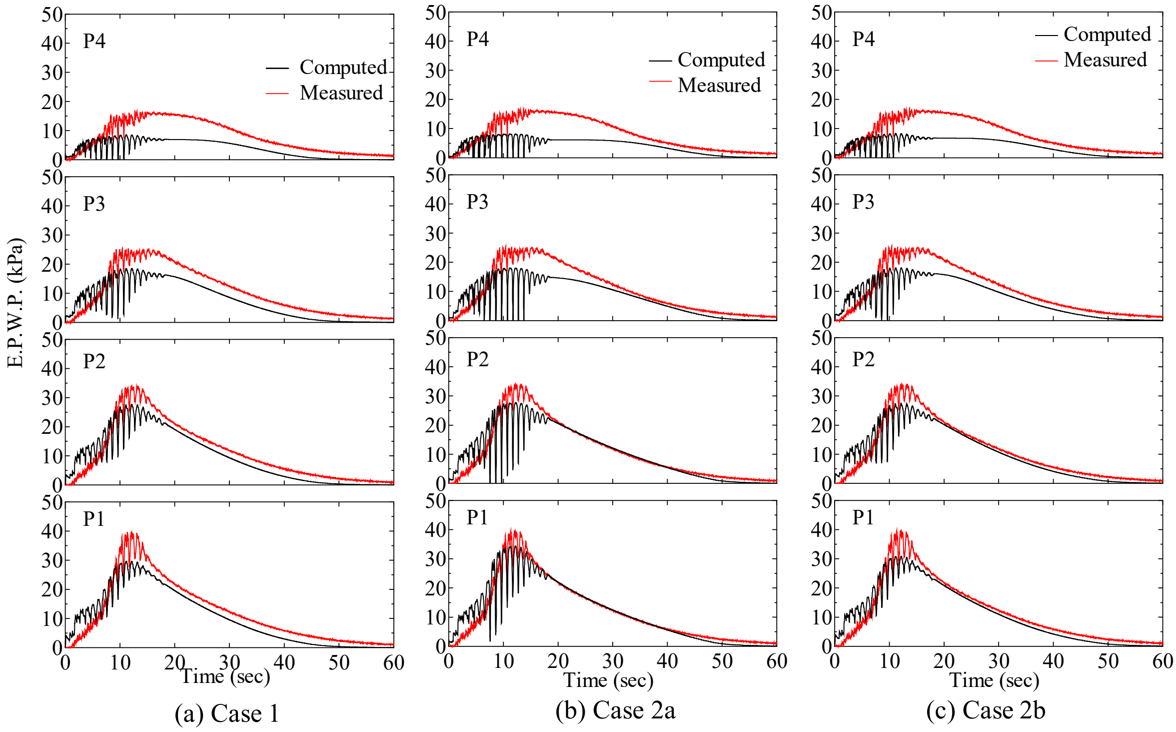

Figure 15 Computed time history of excess pore water pressure for KyU Centrifuge (LEAP-GWU-2015): (a) Case 1; (b) Case 2a; (c) Case 2b

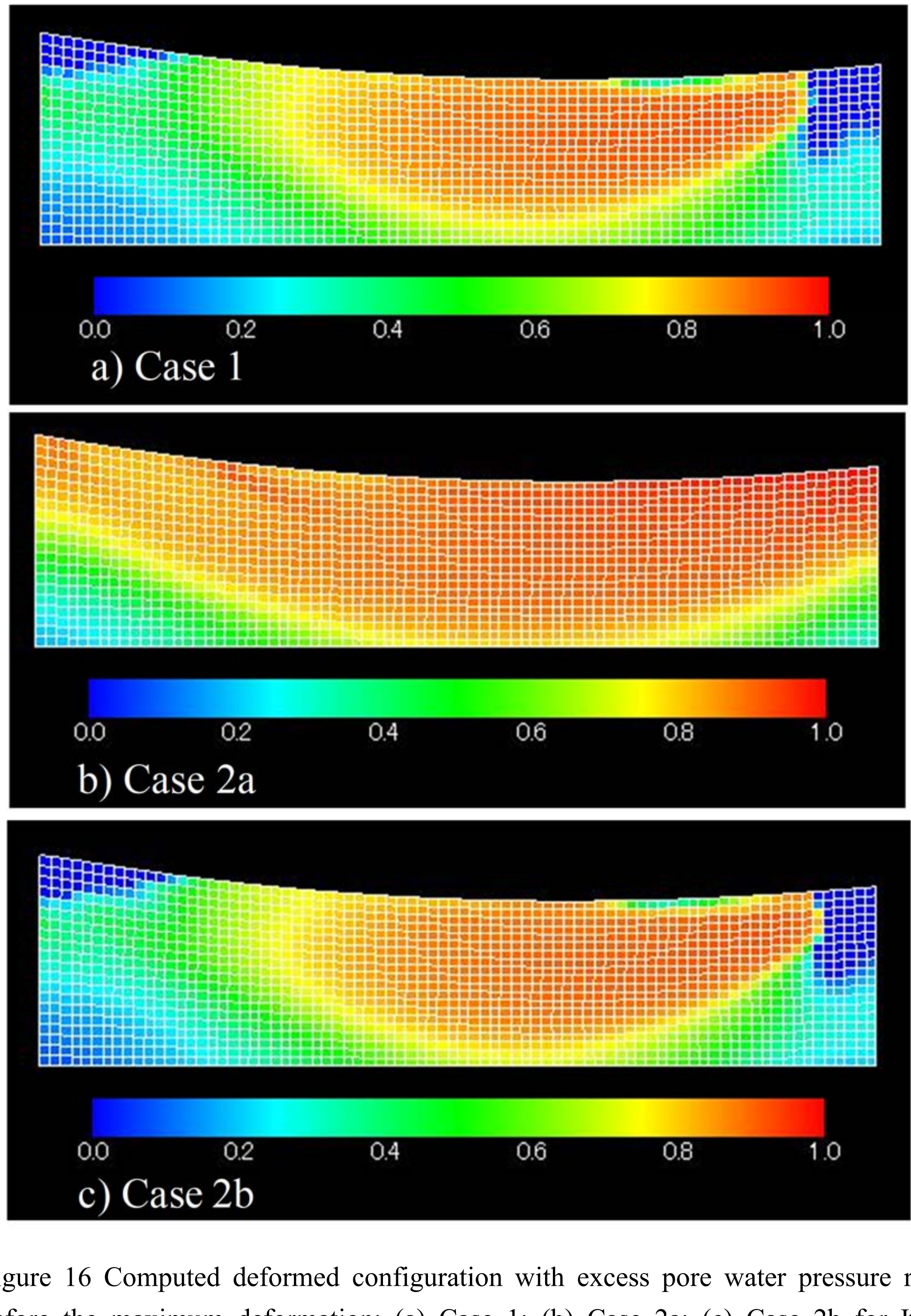

Figure 16 Computed deformed configuration with excess pore water pressure ratio before the maximum deformation: (a) Case 1; (b) Case 2a; (c) Case 2b for KyU Centrifuge (LEAP-GWU-2015)

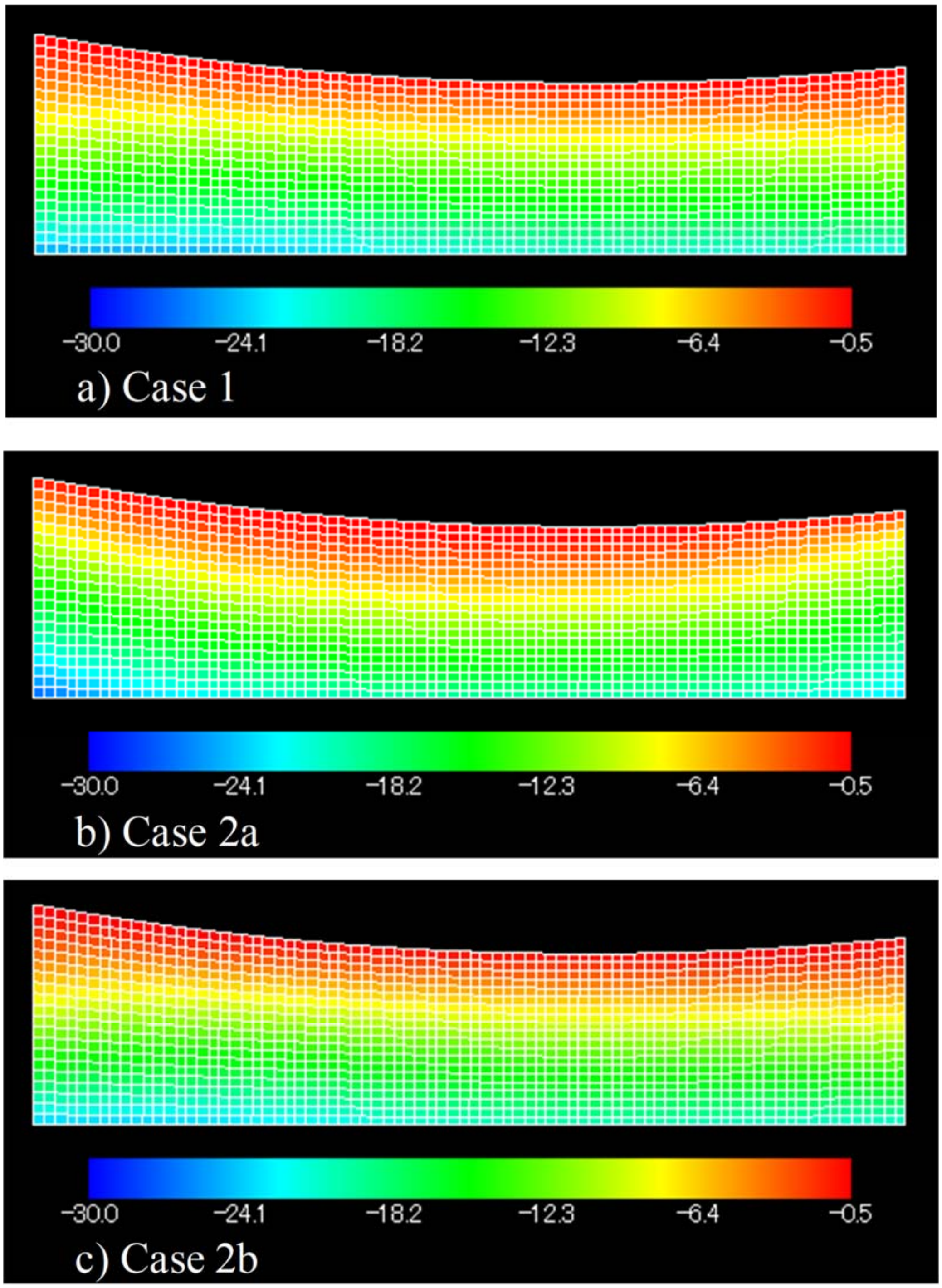

Figure 17 Computed deformed configuration with lateral stress at the end of self-weight analysis: (a) Case1; (b) Case2a; (c) Case2b for UCD Centrifuge (LEAP ASIA2019).

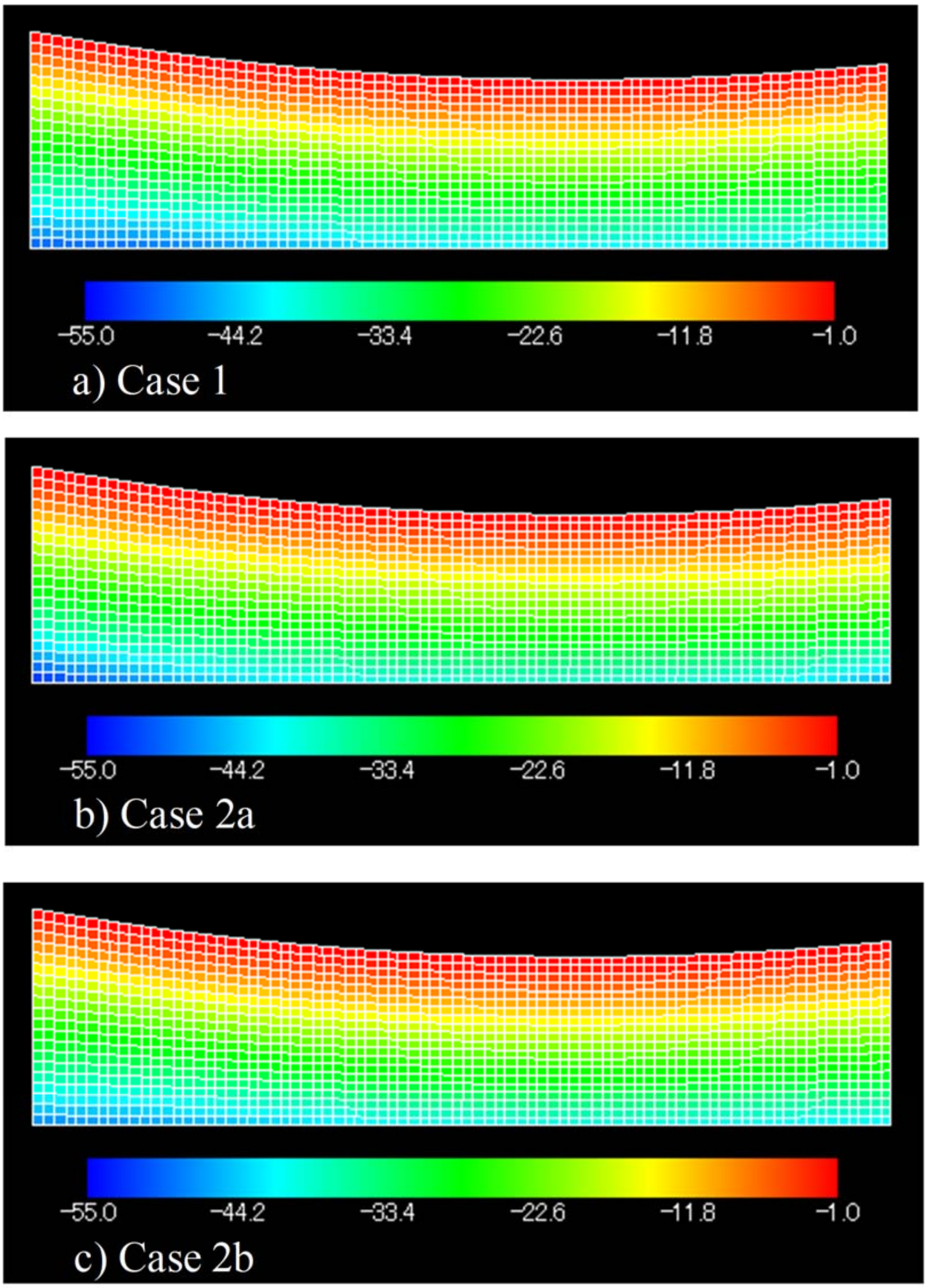

Figure 18 Computed deformed configuration with vertical stress at the end of self-weight analysis: (a) Case 1; (b) Case 2a; (c) Case 2b for UCD Centrifuge (LEAP-ASIA-2019)

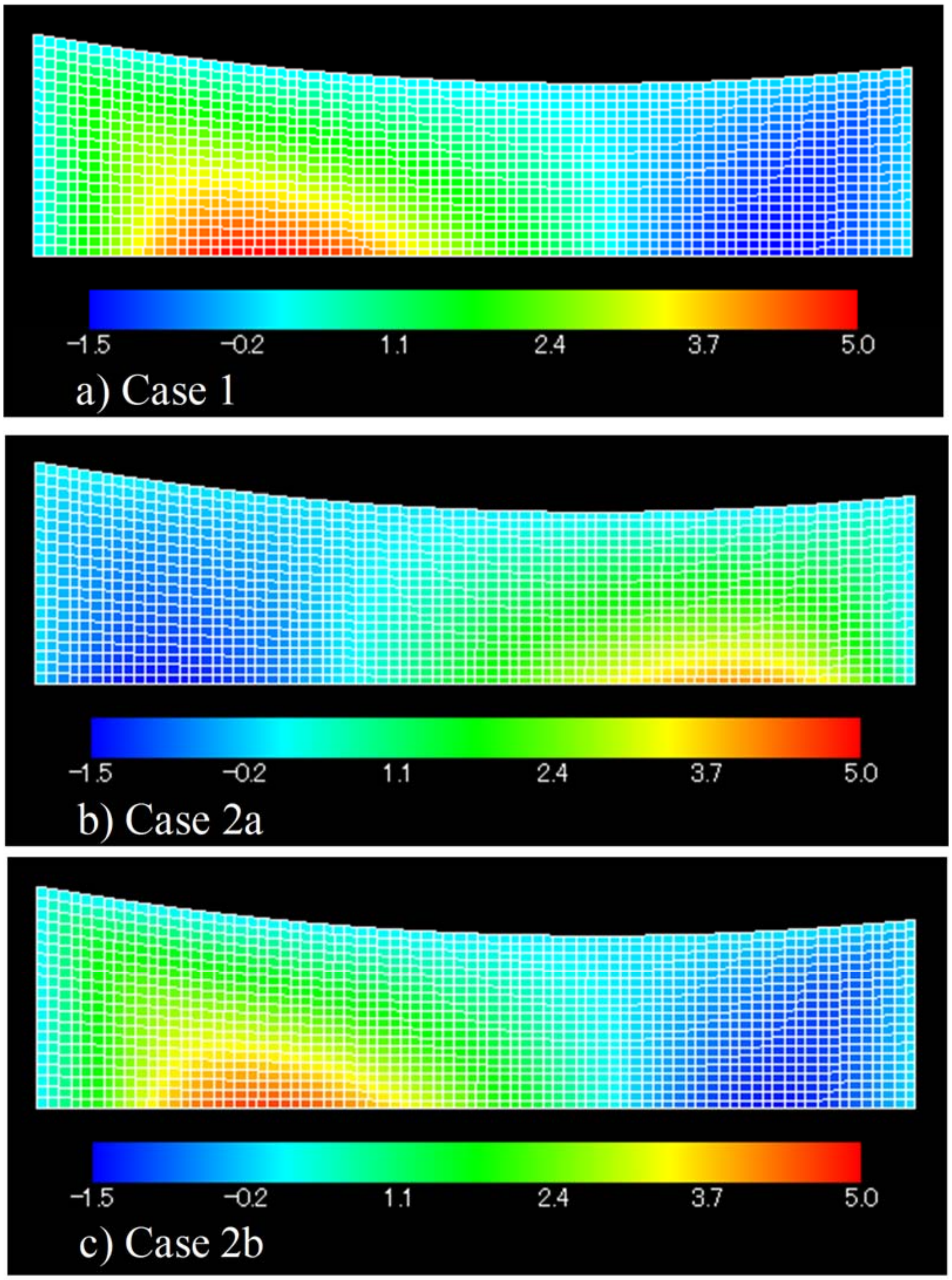

Figure 19 Computed deformed configuration with shear stress at the end of self-weight analysis: (a) Case 1; (b) Case 2a; (c) Case 2b for UCD Centrifuge (LEAP-ASIA-2019)

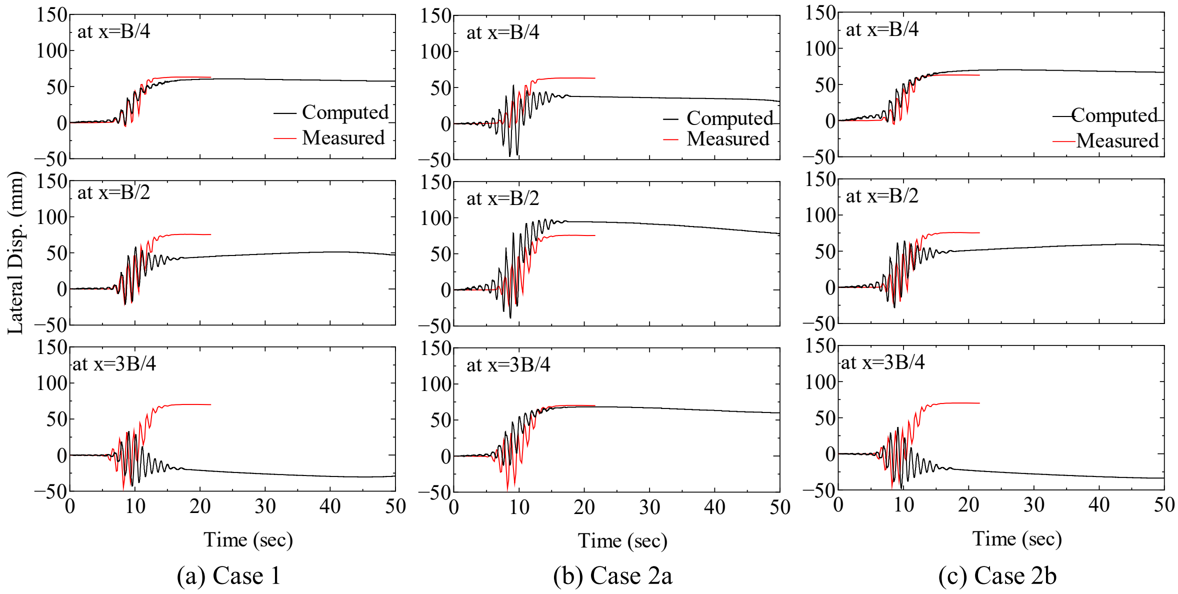

Figure 20 Computed time history of lateral displacement for UCD Centrifuge (LEAP-ASIA-2019): (a) Case 1; (b) Case 2a; (c) Case 2b

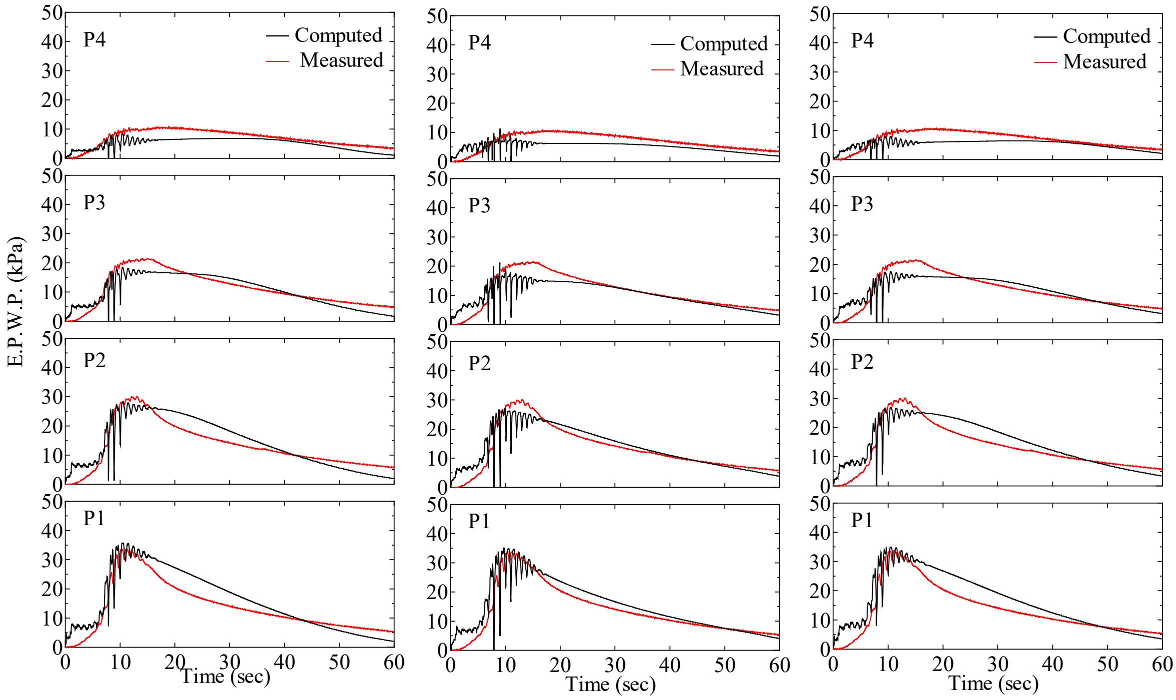

(a) Case 1 (b) Case 2a (c) Case 2b

Figure 21 Computed time history of excess pore water pressure for UCD Centrifuge (LEAP-ASIA-2019): (a) Case 1; (b) Case 2a; (c) Case 2b

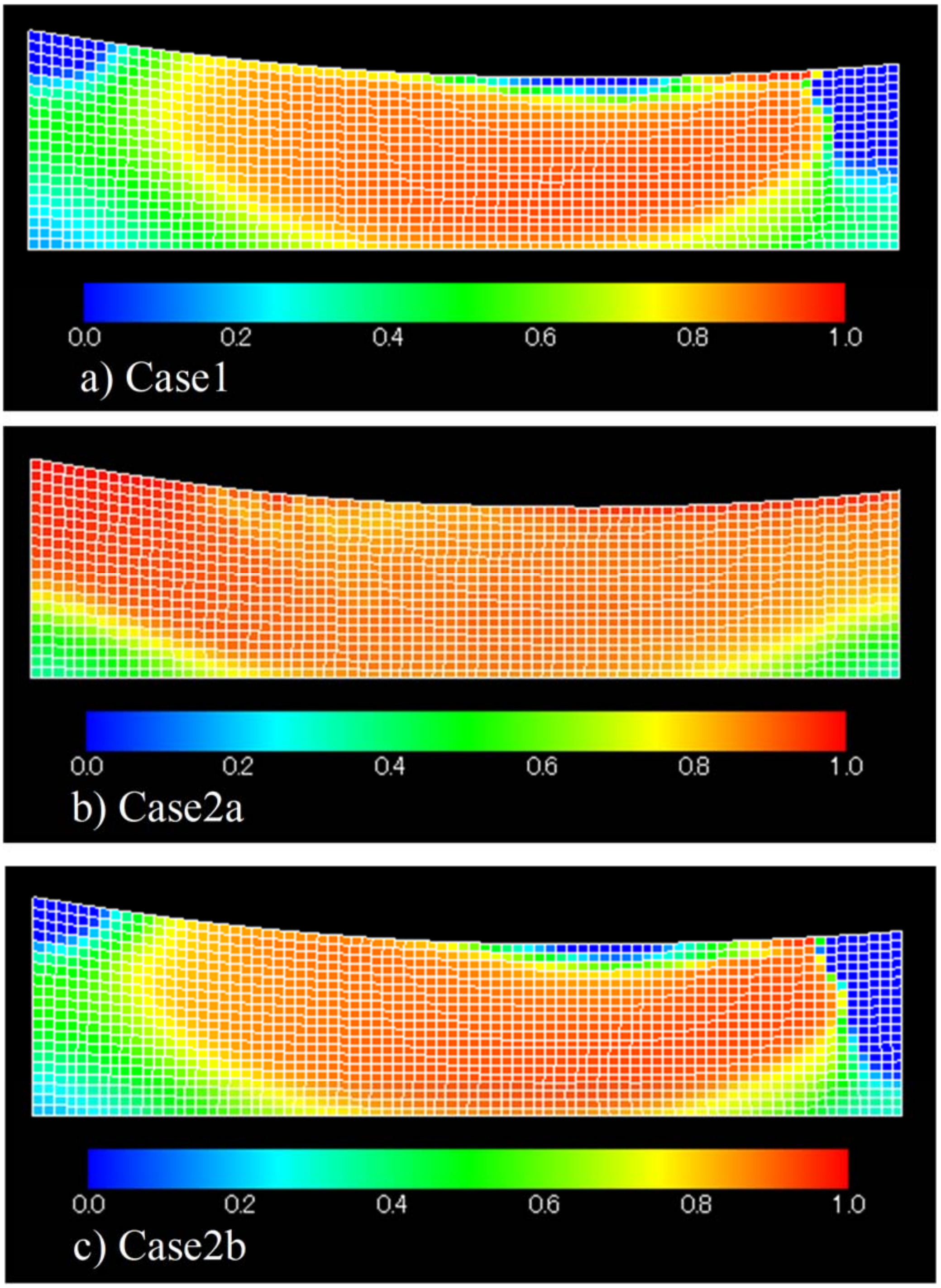

Figure 22 Computed deformed configuration with excess pore water pressure ratio before the maximum deformation: (a) Case 1; (b) Case 2a; (c) Case 2b for UCD Centrifuge (LEAP-ASIA-2019)

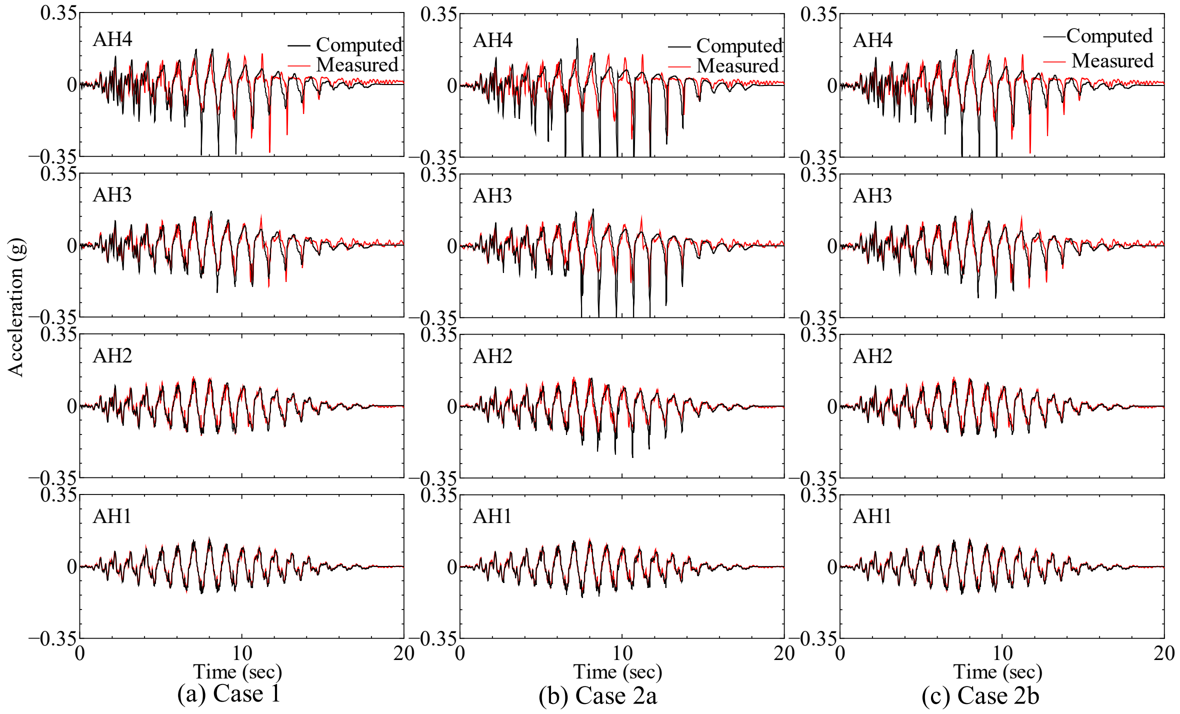

Figure A1 Computed time history of horizontal accelerations for KyU Centrifuge (LEAP-GWU-2015): (a) Case 1; (b) Case 2a; (c) Case 2b

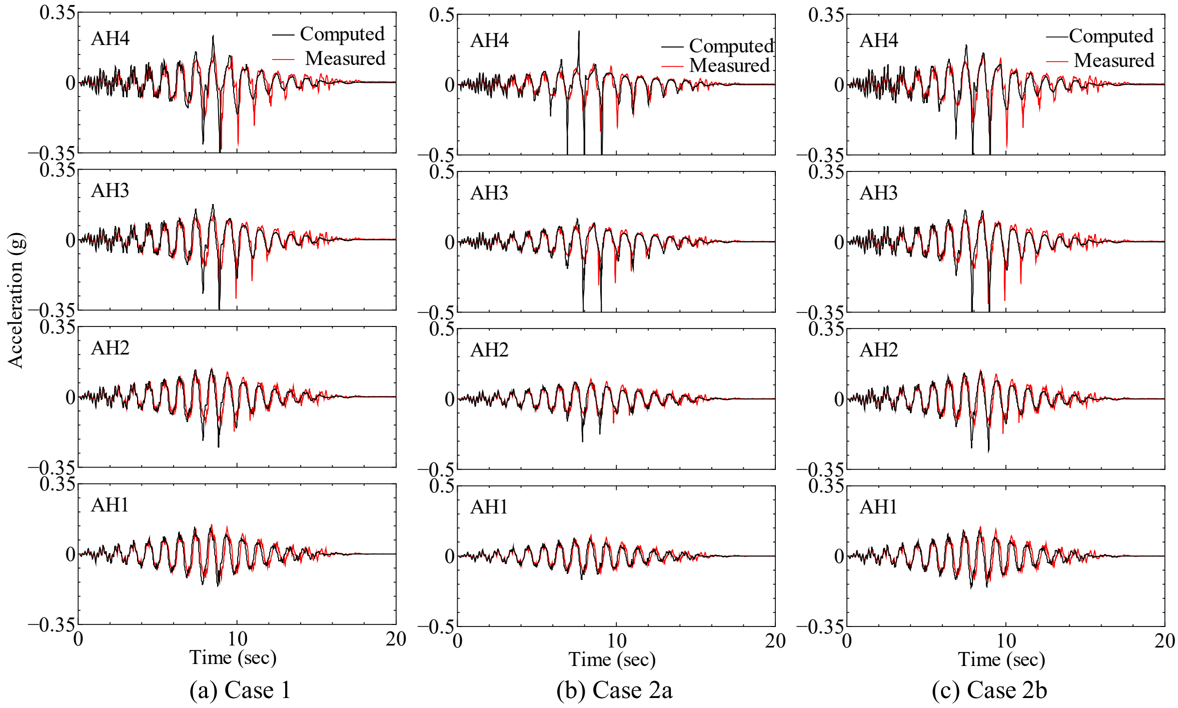

Figure A2 Computed time history of horizontal accelerations for UCD Centrifuge (LEAP ASIA-2019): (a) Case 1; (b) Case 2a; (c) Case 2b